DESIGN AND MANUFACTURING OF A MULTI-DEGREE OF FREEDOM HIP EXOSKELETON FOR BALANCE ASSISTANCE

A Thesis
Presented to
The Academic Faculty

By

Max Anderton

In Partial Fulfillment
of the Requirements for the Degree
Master of Science in the
College of Engineering
School of Mechanical Engineering

Georgia Institute of Technology

May 2022

DESIGN AND MANUFACTURING OF A MULTI-DEGREE OF FREEDOM HIP EXOSKELETON FOR BALANCE ASSISTANCE

Thesis committee:

Dr. Gregory Sawicki
Mechanical Engineering
Georgia Institute of Technology

Dr. Anirban Mazumdar
Mechanical Engineering
Georgia Institute of Technology

Dr. Aaron Young
Mechanical Engineering
Georgia Institute of Technology

Date approved: April 25, 2022

'Why climb Mount Everest?' Because it's there.

George Mallory

ACKNOWLEDGMENTS

did most of the 3D printing for prototyping and strut reinforcement.

Lastly, I would like to thank my friends and family who supported me throughout my life and time here. My mom, dad, brother, grandfather, Auntie Kate, and Uncle Dan were always interested to hear me talk about my project. My friends made my time in grad school outside of research a great experience. Special thanks to Andrew Morganstern for rooming with me for 3 semesters and getting my time in Atlanta off to a good start and Christian Garcia for providing free strength training lessons. Further thanks, in no particular order, to Alex Walen, Alex Rice, Mitchell Tozian, Fabian "Paradise" Pacheco, Krista Kemp, Jake Gullege, Elijah Walen, Lexi Priest, Reo Kunori, Jacob Bultman, Rosario Garcia-Chinchilla, Kyle Bechakas, Zach Beller, Alex Bogaev, and Caleb.

TABLE OF CONTENTS

LIST OF TABLES

LIST OF FIGURES

LIST OF ACRONYMS

2-DOF Two Actuated Degrees of Freedom

AP Anterior-Posterior

FEA Finite Element Analysis

ML Mediolateral

OTS Off-the-Shelf

QDD Quasi-Direct Drive

RMS Root-Mean-Square

ROM Range of Motion

SEA Series Elastic Actuator

UTS Ultimate Tensile Strength

SUMMARY

Lower limb exoskeletons are becoming a more common tool for mobility assistance. While many assist in walking by decreasing metabolic cost, few exoskeleton designs focus on assisting with dynamic stability. Reducing metabolic cost is important, but impaired users must maintain balance to utilize exoskeleton assistance. One of the most important strategies in maintaining balance while walking is to control foot placement using multi-degree of freedom rotation of the hip joint. A hip exoskeleton must be actuated in both the sagittal and frontal planes to help in foot placement by providing swing phase torque for hip flexion/extension and abduction/adduction. The few hip exoskeleton designs that focus on user stability by including actuation in both sagittal and frontal planes (2-DOF), made sacrifices in weight and practicality to provide high levels of assistance.

This thesis puts forward a novel 2-DOF hip exoskeleton design aimed at a lower level of assistance, appropriate for swing phase only, to reduce the exoskeleton's complexity and weight while maximizing its responsiveness. The actuators powering the assistance are quasi-direct-drive and have a high torque to weight ratio. By being backdriveable, these actuators provide mechanical transparency and ensure responsiveness during use. Beyond actuators, the exoskeleton incorporates strategic mechanical decisions to minimize weight. This thesis explores reinforcing 3D printed parts with carbon fiber tape as a replacement for traditional carbon fiber casts. Material tests on reinforced specimens show that it is a legitimate prototyping alternative to conventional carbon fiber layups. Finally, component geometry is optimized to avoid oversized parts while maintaining safety factors for expected stresses. The resulting design represents a 2-DOF powered hip exoskeleton template for testing control algorithms that affords hip-driven, stability assistance during walking.

CHAPTER 1

INTRODUCTION

Balance is an essential skill that many take for granted until it deteriorates due to musculoskeletal impairment from disease or natural aging. Reduced balance leads to a increased risk of falling. Almost two fifths of adults over the age of 70 experience a fall every year [1]. 14% of stroke patients report falling one month after being discharged [2]. Falls can cause significant injuries that could lead to physical and emotional impairment or even death [3]. Furthermore, just the fear of falling has a big negative impact on one's life [4].
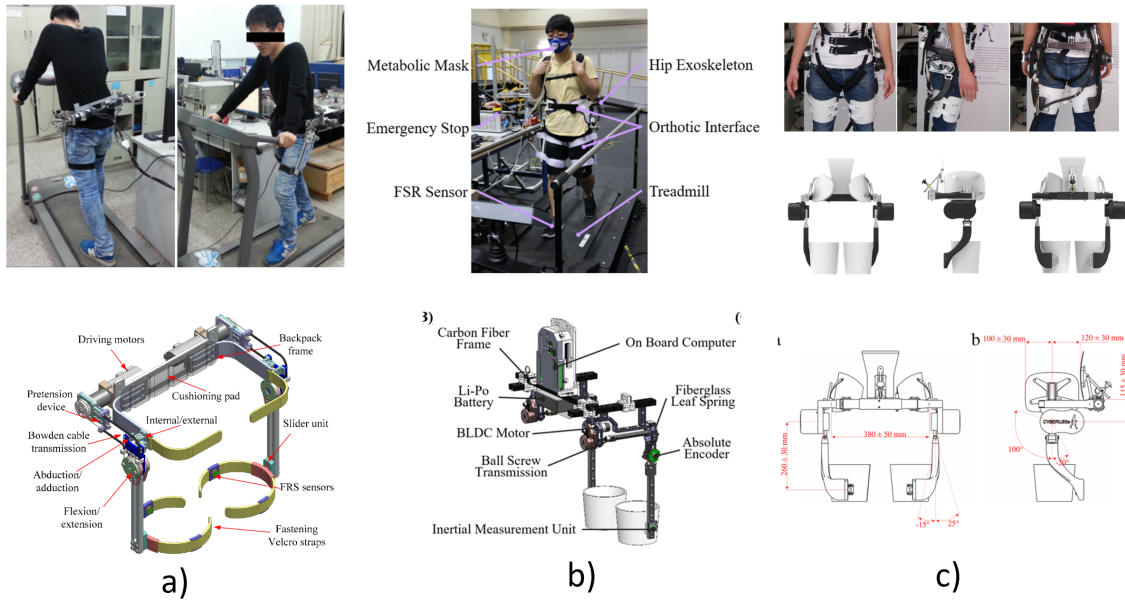
Figure 1.1: Metabolic focused hip exoskeletons. (a) Powered hip exoskeleton (PH-EXOS). Actuated using Bowden cables connected to electric motors [5]. (b) Exoskeleton focused on measuring the effect of hip assistance levels on users' metabolic cost while walking. Uses a ball screw actuator to provide torque to the sagittal plane of the hip [6]. (c) Lightweight active pelvis orthosis (APO). Uses a light-weight SEA unit for actuation [7].

Falls most often occur while walking [8]. As a result, significant research focused on improving the balance and stability of at-risk groups while walking. For example, increasing hip muscle strength with resistance exercise training. The hips apply torque to change

the position and velocity of the body's center of mass as well as control foot placement, and both of these functions are vital to controlling balance during walking [9]. Therefore, hip exoskeletons can be designed to help the user with balance; however, many hip exoskeletons (Figure 1.1) have focused on enhancing human walking and running economy by reducing metabolic cost [10]. Increasing the torque applied to the hip joints while following human movement along with decreasing the exoskeleton's weight will decrease the metabolic cost of a movement [5, 10]. While the hip joint has 3 degrees of freedom as seen in Figure 1.2, the majority of the metabolic cost for hip actuation comes from flexion/extension which is in the sagittal plane [5]. As a result, there are many examples of hip exoskeletons that forgo actuating the frontal and transverse planes when the goal is to minimize metabolic cost [5, 11, 12].
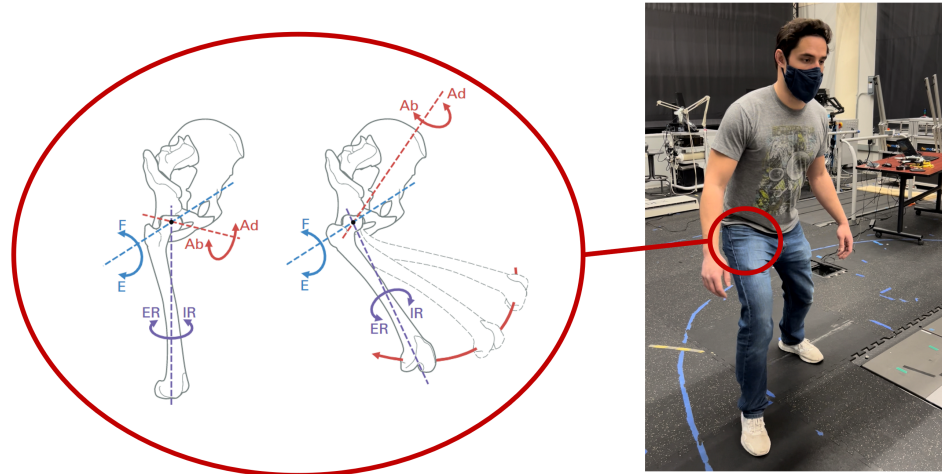
Figure 1.2: Use of foot placement in regaining balance. Movements shown are flexion/extension (F/E), abduction/adduction (Ab/Ad), and internal/external rotation (ER/IR). Hip joint diagram procured through creative commons from [13].

Although it may not be a significant target for minimizing metabolic cost, hip abduction/adduction, which is in the frontal plane, is important when it comes to balance, or more specifically mediolateral (ML) stabilization [14]. Walking is dynamically unstable in the ML direction while naturally stable in the anterior-posterior (AP) direction; therefore, ML foot placement is used by the body to actively stabilize against perturbations in the

same direction while the same is not necessary for AP perturbations [15]. ML instability generally increases with age [16] and can also result from stroke [17], which makes those groups increasingly susceptible to falling [18]. This is not to say that hip flexion/extension is not important in balance. In fact, standing is more unstable in the AP direction [15], but dynamic stability relies most heavily on ML corrections.

As a result, there has been increased interest in actuating both frontal and sagittal planes of the hip joint in recent years. Many exoskeletons that actuate the hip in the frontal and sagittal plane also actuate the knee and ankle [19]. While this is important for more expansive goals, such as restoring the ability to stand and walk, it is less critical for reducing fall risk and adds complexity and weight to any potential design. There are a few examples of exoskeletons that focus mainly on the frontal and sagittal planes of the hip joint which can be called 2-DOF hip exoskeletons (Figure 1.3).
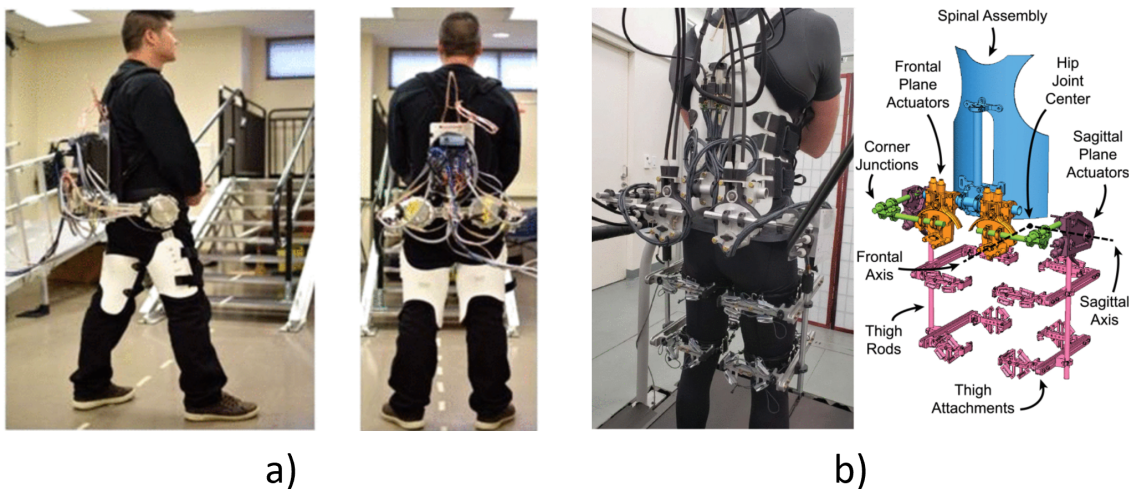
Figure 1.3: Examples of 2-DOF Hip Exoskeletons. (a) Zhang *et al.* exoskeleton. First example of a 2-DOF exoskeleton. Was focused on improving user balance over reducing metabolic cost. Actuated using SEAs [20]. (b) Chiu *et al.* exoskeleton. Uses off board motors connected with Bowden cables to actuate multi-DOF hip exoskeleton frame [14].

The first notable 2-DOF hip exoskeleton came from Zhang *et al.* (Figure 1.3(a)) which generated up to 50% of biological torque required for normal walking with a series elastic actuator (SEA) while keeping its weight limited to 9.2 kg (excluding battery) and being autonomous of a tethering system [20]. SEAs are mechanically safer and can be geared

higher than traditional actuator setups while remaining backdriveable [21], but they come with sacrifices in control bandwidth performance, added complexity, increased mass, and increased size for the system, which limits their usefulness for wearable robotics [22].

Chiu *et al.* developed a 2-DOF hip exoskeleton (Figure 1.3(b)) that provided up to 68% of biological torque at 10.9 kg but was tethered [14]. Tethered designs are good for testing purposes, since they offload the actuators and batteries which reduce the weight on the user, but a tether is not practical for everyday use.

For the purpose of restoring gait stability, potential users, like the elderly and stoke patients, require a design that prioritizes being responsive and practical for everyday use. This thesis seeks to achieve those broad design goals by using less powerful motors than other designs. For one, this exoskeleton uses quasi-direct drive (QDD) motors to allow for backdriveabilty without the sacrifices that come with SEAs. Furthermore, this exoskeleton is not tethered thereby allowing for autonomous use. As secondary goals, we sought to minimize complexity to make manufacturing and revisions easier to handle. Most of the reductions in complexity resulted from identifying alternatives to carbon fiber interface designs. One such example is the reinforcement of 3D printed parts with carbon fiber tape on the exoskeleton's leg struts. This alternative to traditional carbon fiber parts is an effective prototyping solution for light weight but strong components. Material tests validate that the reinforcing process is sufficient for the stresses expected on the leg struts.

This thesis is organized as follows. Chapter 2 fleshes out the design objectives of the exoskeleton. Chapter 3 describes the mechanical design along with additional information on manufacturing methods. Chapter 4 discusses the results of the prototype and suggests potential future work. Chapter 5 synthesizes the conclusions made from the finalized design.

CHAPTER 2

EXOSKELETON DESIGN REQUIREMENTS

The exoskeleton put forth in this thesis serves as a proof of concept and a framework for further research and development, and it is not intended for everyday use. With this in mind, this Chapter describes the requirements of the design in order to achieve its goal as a platform for fast design iteration.

2.1 Actuator Requirements

To assist in gait stability while walking, the exoskeleton must actuate the user's hip joint in both the frontal and sagittal plane to help with step-width adaption and foot placement. To do this, the actuators must provide enough torque to assist the user in lateral stability at a rotational speed high enough to match natural movement of the hip joint. These requirements for a potential actuator can be split up into sagittal and frontal planes since hip flexion/extension and ab/adduction serve two very different roles in gait stabilization.

The rotational speeds required by the frontal and sagittal actuators are based off the maximum angular velocity that the hip joint would rotate in each plane respectively. For both planes, the hip joint will experience higher angular velocities when perturbed in comparison to normal walking. An extreme example of this would be evading obstacles. Moolchandani *et al.* found that rapid evasions in a series of different directions elicited rotational velocities up to 7.5 rad/s (≈75 rpm) and 5 rad/s (≈50 rpm) in the sagittal and frontal planes respectively (Figure 2.1) [23].

To find the goal peak torque required to assist in stabilization, the torque required while walking should be analyzed. The peak sagittal hip torque during normal walking occurs during left or right initial contact (≈50% or ≈100% gait cycle) and has a peak torque of around 1.40 Nm/kg [24], which equates to around 130 Nm for a 90 kg user. Naturally, the
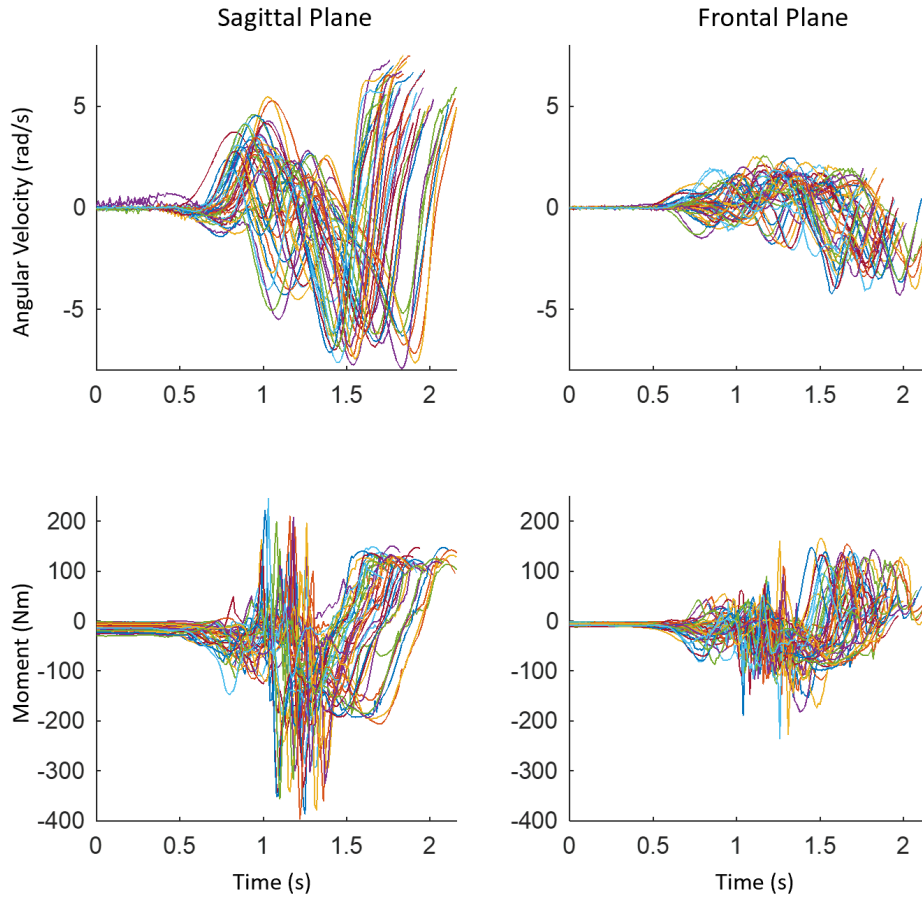
Figure 2.1: Hip biomechanics while dodging obstacles in a series of different directions. Different color lines represent different participants in the study [23].

torque required to regain balance can be more than that which is required to walk. Peak torque during a slip perturbation was found to be around 135 Nm [25]. Moolchandani *et al.* recorded hip flexion torques up to 400 Nm during AP evasions (Figure 2.1).

The peak frontal hip torque during normal walking occurs after contralateral toe-off ($\approx$10% gait cycle) and, according to one study, is around 1.63 Nm/kg for healthy individuals [26]. This would equate to around 150 Nm for a 90 kg user. Other kinds of perturbations require higher hip torques on average to stabilize the COM. For example, when laterally perturbed at the pelvis, one study found that older adults would generate up to around 2.2 Nm/kg of abduction torque to stabilize the body in the mediolateral direction with protective stepping [27], and this would equate to around 200 Nm. The extreme of this would

again be when a user is rapidly evading. Moolchandani *et al.* recorded adduction up to 250 Nm when evading in the ML direction (Figure 2.1) [25].

Table 2.1: Peak angular speed and torque of the hip joint from different studies.

Plane	Scenario	Peak Angular Speed (ω)	Peak Torque (τ)	Source
	Steady State	43 rpm	108 Nm	[25]
Sagittal	20% Slip	48 rpm	135 Nm	[25]
	AP Evade	75 rpm	400 Nm	[23]
Frontal	Steady State	x	130 Nm	[24]
	ML Evade	50 rpm	250 Nm	[23]

A summary of the different peak hip angular velocities and torques is shown in Table 2.1. The extreme values of this were used to set ideal goal torques for an actuator assisting in gait stabilization (Table 2.2). However, selecting an actuator cannot be based only on the required peak torque and velocity. Rather, further analysis is required to determine how much torque an actuator can provide without failing. First, Equation 2.1 is used to check the maximum amount of assistance an actuator can provide for different use cases without going over its nominal voltage. Then, the root-mean-square (RMS) torque of this level of assistance over uses cases is checked using Equation 2.2. If RMS torque is calculated to be above the rated torque of the actuator, the assistance is lowered further to prevent the actuator from overheating.

$$V = \frac{\tau * R}{K_t} + K_e * \omega \tag{2.1}$$

where: V = supply voltage [V]

τ = torque [Nm]

R = Armature resistance [Ohms]

K_t = torque constant [Nm/A]

K_e = voltage constant [V/rpm]

ω = angular speed (without gearing) [rpm]

$$\tau_{rms} = \sqrt{\frac{\sum_{n=1}^{s} \tau_n^2 * t_n}{\sum_{n=1}^{s} t_n}} \qquad (2.2)$$

where: τ_{rms} = RMS Torque [Nm]

s = Number of segments

τ_n = Torque at segment n [Nm]

t_n = Duration of segment n [s]

While providing a high level of mechanical assistance is important, there are some other aspects to take into account when selecting an actuator. For one, lightweight actuators can help meet the design's low weight goal. Furthermore, an actuator that is backdriveable is needed to make an exoskeleton that is mechanically transparent and responsive to user input. To be comfortably backdriveable, the actuator selected must be QDD and have a gearing ratio $\leq$ 10:1 [28].

Table 2.2: Hip actuator design goals. Peak torque and velocity values taken from the extreme values shown in Table 2.1.

Actuator Goals	Goal Values	
	Sagittal	Frontal
Peak Torque	400 Nm	250 Nm
Peak Velocity	75 RPM	50 RPM
Reduction Ratio	Maximum 10:1	

2.2 Interface Requirements

The exoskeleton's interface should be able to be used by a wide range of users safely and comfortably. In terms of compliance, the exoskeleton should accommodate the hip width, hip separation, and other anthropometric features in the range of 25% to 95% of the adult population as detailed in [29] (Figure 2.2). Keeping the mass of the exoskeleton low is important to reduce metabolic cost that comes with adding worn mass to the user as well as minimizing discomfort. Therefore, a goal weight of 9 kg was set for the design's weight

so that it would be lighter than previously published 2-DOF designs.
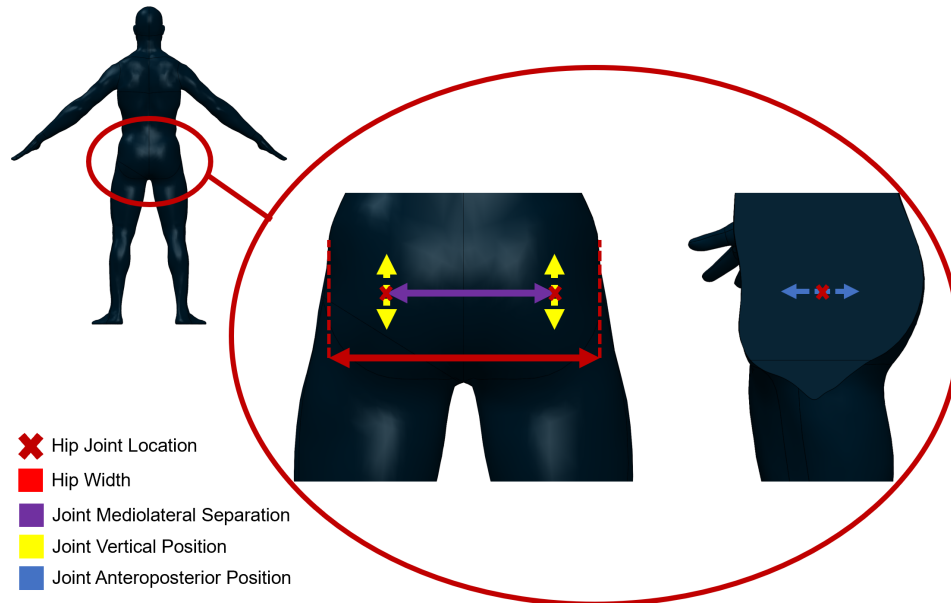
Figure 2.2: Important hip anthropometric measurements. The approximate location of the hip joint is shown by a red x. The following are shown: overall hip width (red), mediolateral hip joint separation (purple),the height of the hip joint center (yellow), and the anteroposterior hip joint center position (blue).

Finally, the exoskeleton should handle the range of motion ROM and forces that occur during steady walking and perturbation responses. The maximum hip flexion/extension and ad/abduction recorded during walking is around $+40°/-10°$ and $+6°/-10°$ respectively [30]. For trip perturbations,the maximum hip flexion/extension and ad/abduction averages around $+52°/-13°$ and $+7.4°/-5.2°$ respectively [31]. Since it is important that the user's movement is not over restricted, and having excessive range of motion has few drawbacks, this thesis adds $20°$ of range to each motion rounded up to the nearest $5°$ to account for any deviation from the averages. Therefore, the resulting goal hip flexion/extension and ad/abduction angles are $+75°/-35°$ and $+25°/-30°$.

CHAPTER 3

DESIGN IMPLEMENTATION

The exoskeleton (Figure 3.1) described in this thesis can apply torque in the frontal and sagittal planes of the user's hip joint to assist in hip ad/abduction and flexion/extension. Four backdriveable motors are directly connected to the user through the exoskeleton's interface. The exoskeleton provides low level torques across a broad range of speeds but is primarily designed for walking.

Figure 3.1: Assembled hip exoskeleton without mechatronics. Front (left), side (middle), and back (right) views of the exoskeleton.

3.1   Exoskeleton Actuation

The need to be backdriveable, responsive, and lightweight limits the torque output of a conventional actuator. While approaching 100% biological hip torque would be ideal, an exoskeleton doesn't need such high torques to assist during swing phase to help apply corrective foot placement (i.e. step width/length). Previous balance focused 2-DOF hip exoskeletons had continuous torques around 40 Nm and peak torques around 80 Nm in

both planes which resulted in significant improvements in gait stability for healthy users
[14, 20]. While these results are promising, those exoskeleton designs made sacrifices
mentioned earlier to achieve higher torque. To be backdriveable and responsive, potential
actuators must be QDD and therefore will have lower torque outputs than previous 2-DOF
designs. While it has shown promise for other exoskeleton designs [11], a custom built
actuator designed for high torque low gearing applications was outside the scope of this
project and the decision was made to stick with off-the-shelf (OTS) solutions.

The market for QDD, high torque weight ratio actuators is niche and this severely lim-
ited the options for the design. While many others were explored, the options were nar-
rowed down to T-motor's newly released AK Series Dynamical Modular actuators which
are all QDD with compact, integrated planetary gears which maximizes their torque to
weight ratio. Within this series, the AK80-6, AK80-9, AK70-10 , and AK10-9 (V1.1) are
compared (Table 3.1).

Table 3.1: Actuator specification comparison. 24 V versions of the AK70-10 and AK10-9
were excluded. Data provided by Tmotor.

Actuator	Weight	Voltage	Rated/Peak Torque	Rated Speed	Rated/Peak Current	Max Torque Weight Ratio
AK80-6	485 g	24 V	6/12 Nm	365 rpm	12/24 A	24 Nm/kg
AK80-9	485 g	24 V	9/18 Nm	245 rpm	12/24 A	37 Nm/kg
AK70-10	521 g	48 V	8.3/24.8 Nm	400 rpm	8.8/26.1 A	47.6 Nm/kg
AK10-9	820 g	48 V	15/38 Nm	445 rpm	18.5/50 A	65 Nm/kg

Since the highest peak torque of the group, 38 Nm, is below the goal torque to hangdel
both planes, the same actuator is used in both planes for simplicity sake (i.e. 4 identi-
cal motors). Using Equation 2.1, as described in section 2.1, we calculated the maximum
assistance level under different gait scenarios for all actuators (Figure 3.2). These simula-
tion were then checked using Equation 2.2 to make sure RMS torque did not exceed rated
torque. The thesis uses steady state sagittal gait, slip perturbation, AP evasion, and ML
evasion gait scenarios for analysis.

A comparison of the actuators based on their voltage-limited assistance levels shows
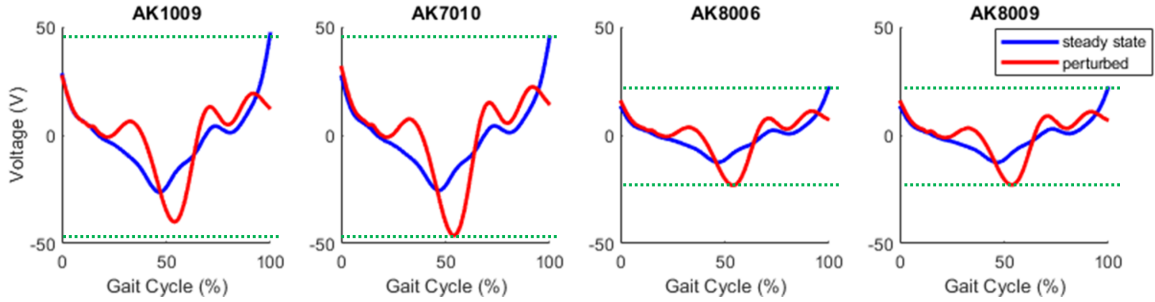
Figure 3.2: Required actuator voltage during steady state and perturbed gait for maximum assistance without failure. Voltage is based off what each actuator outputs (Equation 2.1). The maximum voltage of each motor is represented by the green lines. The AK 10-09's perturbed trial is limited by RMS torque (Equation 2.2) rather than its maximum voltage. Steady state and perturbed data are based off sagittal biomechanics data [25].

that the AK10-9 leads the pack in terms of percent biological torque for steady state and different examples of perturbed gaits (Figure 3.3). However, even though it has the highest torque-to-weight ratio, the AK 10-9 is too heavy, at 820 g, for the design's weight goal of 9 kg since just four of those actuators would weigh 3.3 kg. Therefore, the AK 70-10 is used because it weighs much less, at 521 g, while providing a respectable amount of assistance. Further analysis of the AK70-10 for swing phase specific assistance is shown in Appendix A.
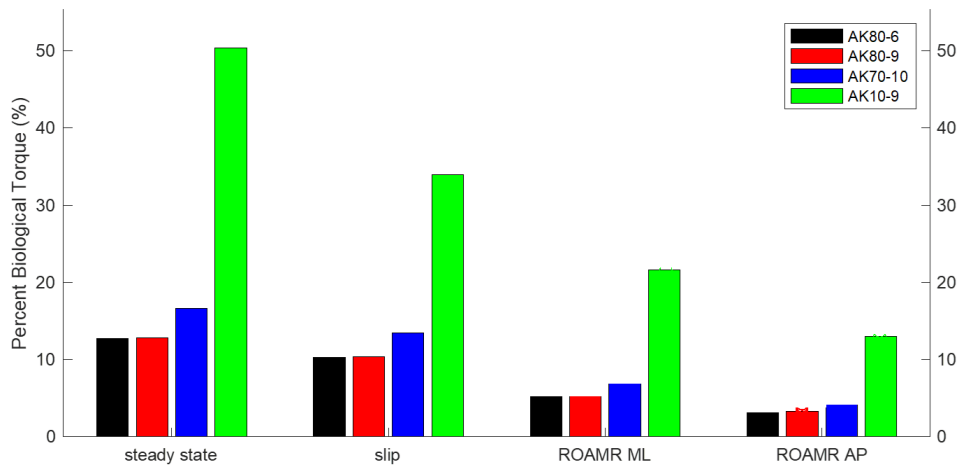
Figure 3.3: Assistance comparison of different actuators during normal and perturbed gait. Steady state data was based off sagittal biomechanics data [25]. Three perturbation studies were used as different references for levels of assistance each motor could provide: slip perturbations [25], mediolateral (ML) evasions [23], and anteriorposterial (AP) evasions [23].

3.2 Exoskeleton Structural Design

The exoskeleton interface is split up into back, hip, and leg segments (Figure 3.4). With the exception of the leg struts, all custom parts were made with aluminum 7075-T6 due to its high specific strength.
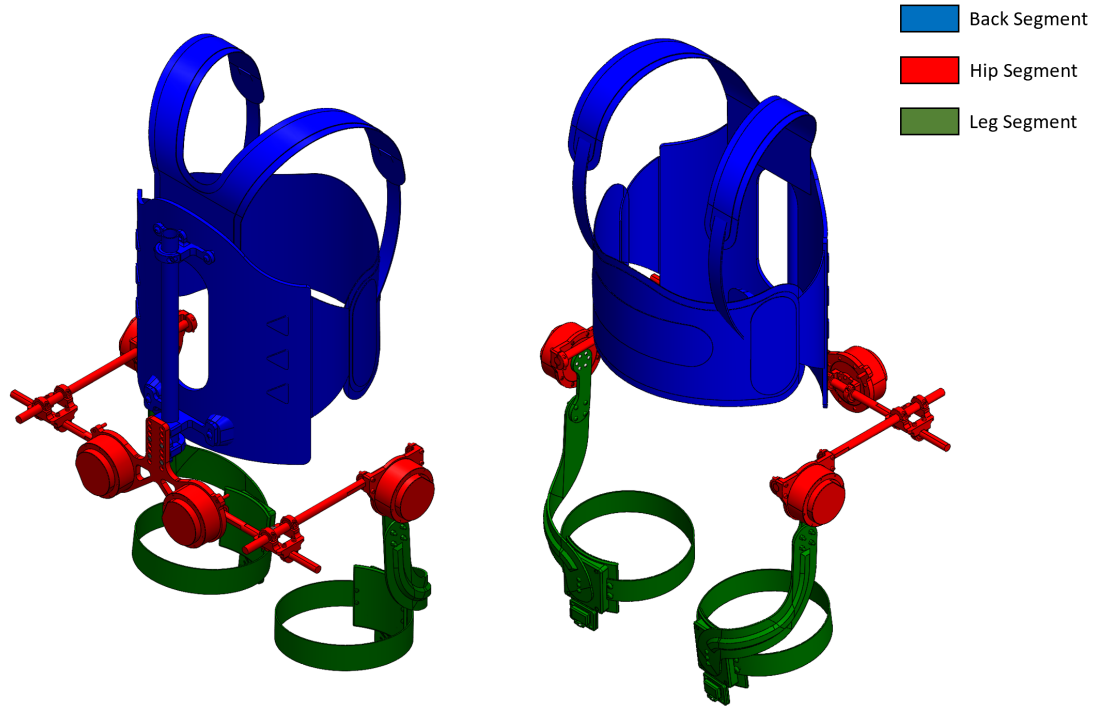
Figure 3.4: Exoskeleton segments. Back (left) and front (right) views of the exoskeleton.

3.2.1 Back Segment

The back segment of the design, as seen in Figure 3.5, consists of the back interface and the hardware which connects it to the hip segment. The back interface needs to provide a secure and rigid foundation for the rest of the exoskeleton interface. An OTS lumbar orthosis (Figure 3.5(a)) was used to achieve these aforementioned goals. A drawback to using an OTS orthosis is that it weighs 1.8 kg which is more than common custom built back interfaces. Originally, we planned to manufacture a carbon fiber back plate, but the complexities in manufacturing and securing a custom back plate were deemed too great.

Figure 3.5: Back segment of the exoskeleton. Assembled (left) and exploded (right) views of the back segment of the exoskeleton. (a) Lumbar orthosis. (b) Hollow aluminum pipe. (c) Epoxy mounds. (d) Connector mount. (e) Dowel pins.

The orthosis connects to the rest of the exoskeleton interface using a hollow aluminum pipe (Figure 3.5(b)) mounted at the top and bottom of the orthosis's back plate. The bottom mounting point required epoxy mounds (Figure 3.5(c)) to make a flat surface for mounting. The connection points to the orthosis are spread out by the pipe to make the exoskeleton more secure. The hollow pipe connects to the hip segment through the connector mount (Figure 3.5(d)). The connector mount has dowel pins (Figure 3.5(e)) press fit into it to allow for easier placement of the frontal motor mount and to take the shear load coming from the hip segment. Much of this assembly is inspired by Chiu's design [14].

3.2.2   Hip Segment

The hip segment contains the mounts for the frontal and sagittal plane motors as well as the structure connecting them as seen in Figure 3.6. The frontal motor mount (Figure 3.6(a)) is designed to be modular in terms of adapting to the femoral head width of the user (Figure 2.2). The frontal motor mount has a range of mounting holes so that its vertical position
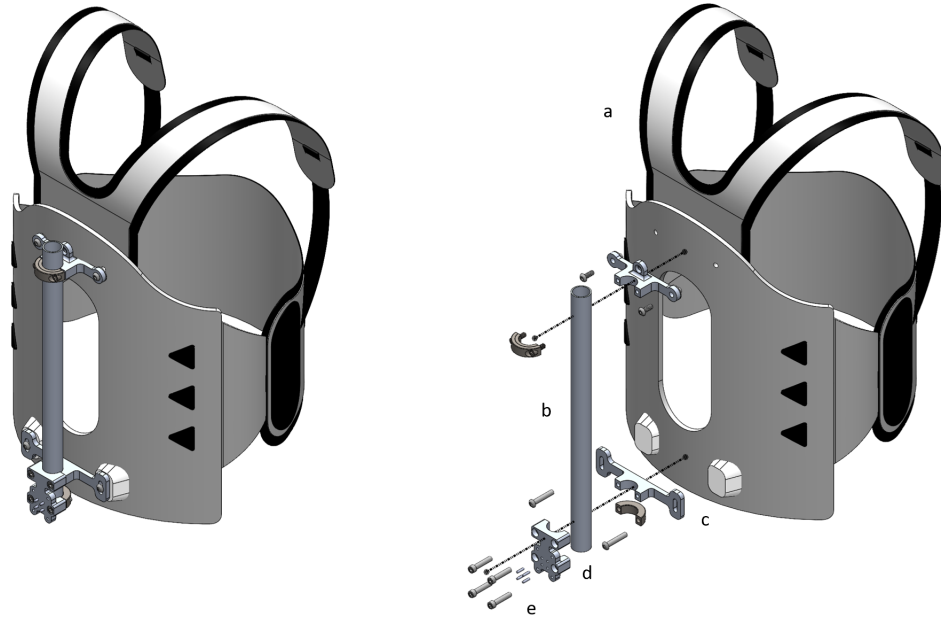
14

Figure 3.6: Hip segment of the exoskeleton. Assembled (left) and exploded (right) views of the hip segment of the exoskeleton. (a) Frontal motor mount. (b) Dowel pin hard stop. (c) Frontal motor. (d) Sagittal Motor. (e) Frontal motor output assembly. (f) L-junction assembly. (g) Sagittal motor mount assembly.

can be changed. There is a dowel pin (Figure 3.6(b)) press fit into the frontal motor mount to act as a 45° hard stop for abduction. The frontal motor (Figure 3.6(c)) connects to the sagittal motor (Figure 3.6(d)) by perpendicularly orientated aluminum rods. Carbon fiber struts were originally planned to connect the frontal and sagittal motors; however, the complexity of manufacturing the carbon fiber parts coupled with the project's timeline meant a simpler solution was needed. The idea to use aluminum rods came from Chiu's design [14]. The aluminum rods have a Dshaft on them to ensure the motors are always mounted parallel to their assigned plane. The frontal motor has an aluminum rod connected at its output (Figure 3.6(e)). The frontal aluminum rod connects with the sagittal aluminum rod at the L-junction assembly (Figure 3.6(f)). The L-junction's shaft clamps secure the aluminum rods and can be loosened to allow the rods to move for adjustment of the sagittal motor's position. The sagittal aluminum rod then connects to sagittal motor mount (Figure 3.6(g)) via clamps.

3.2.3 Leg Segment and Leg Struts

The leg segment connects the sagittal motor to the user's leg as seen in Figure 3.7. The sagittal motor (Figure 3.7(a)) has a connector plate (Figure 3.7(b)) mounted to its output which in turn mounts to the leg strut (Figure 3.7(c)). The leg strut then connects directly to the leg interface (Figure 3.7(d)) which is taken from the Kang *et al*'s design (unpublished). Originally the leg strut was going to be directly connected to the motor, but the connector plate was added to increase the reach of the leg strut by 9 cm so that the leg interface could be mounted closer to the knee. Mounting the leg interface further down the leg reduces the force on the user by increasing the torque arm length.
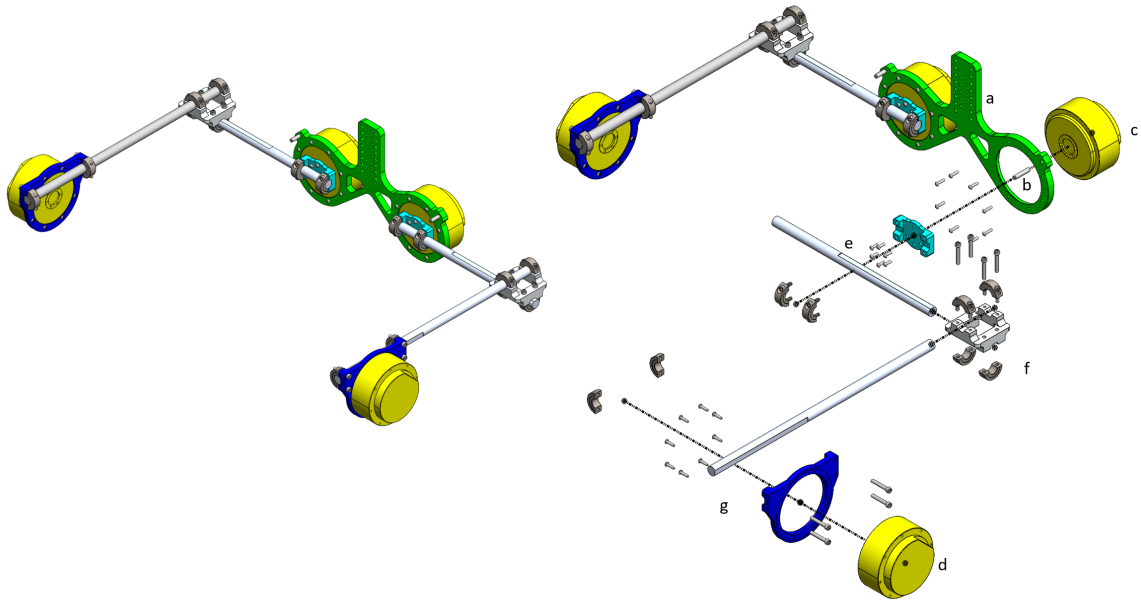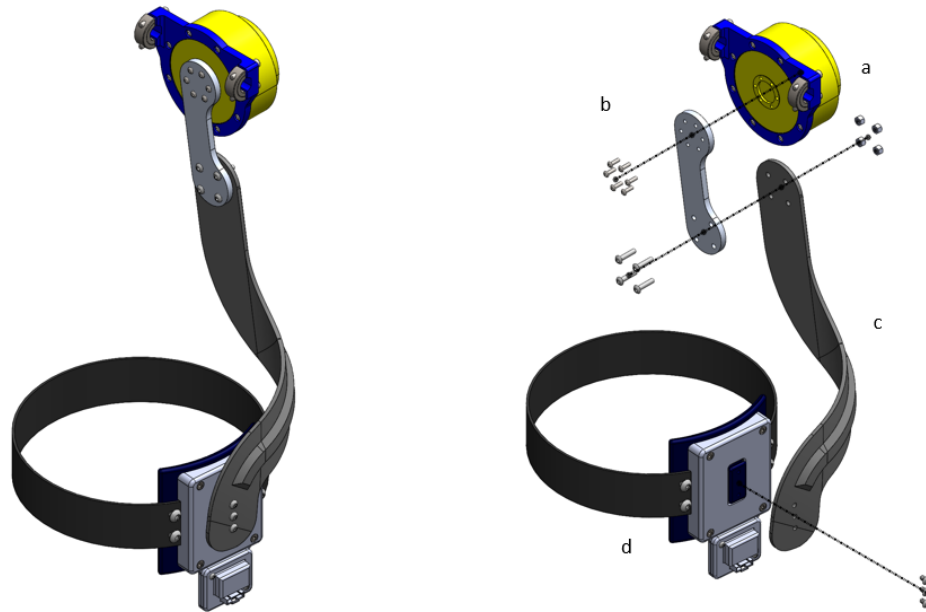

Figure 3.7: Leg segment of the exoskeleton. Assembled (left) and exploded (right) views of the hip segment of the exoskeleton. (a) Sagittal motor assembly. (b) Connector plate. (c) Leg strut. (d) Leg interface.

The leg strut design was based off Kang *et al*'s design (unpublished) in terms of sizing and shape. They needed to be made out of a material with a high strength to weight ratio due to their size and the stresses they would be put under (subsection 3.5.1). Naturally, a carbon fiber composite is considered the best option to achieve this do to its high specific

strength. Therefore, the struts were originally planned to be made using the traditional method of a wet layup; however, this process is very labor intensive and the autoclave required to finish the layup properly was not available during the manufacturing of the design. As an alternative, this exoskeleton uses 3D printed parts reinforced with carbon fiber tape as a less labor intensive option for making prototype parts with high strength to weight ratios. The inspiration for this idea came from the Markforge Mark Two composite 3D printer which applies a carbon fiber skin to its 3D printed parts to reinforce them.

Leg Strut Manufacturing Method

The leg strut base is printed with a carbon fiber reinforced nylon composite on a Onyx One 3D printer (Figure 3.8(a)). This composite material, named Onyx, is used because it offers a higher specific strength than other FDM materials. This base print is then reinforced with carbon fiber tape. 3" wide unidirectional carbon fiber tape is cut to a length equivalent to the leg struts and then lathered with an epoxy solution made of 2 parts resin and 1 part hardener (Figure 3.8(b)). With the epoxy solution applied, the carbon fiber tape is draped longitudinally across one side of the leg strut and stretched to match the curvature (Figure 3.8(c)). This process is repeated so that both sides of the leg struts had two layers of carbon fiber tape. The reinforced leg strut is then vacuum packed in a PVA bag and left to set for around 24 hours (Figure 3.8(d)). Once set, the reinforced leg strut is removed from the PVA bag (Figure 3.8(e)) before being grounded down to remove excess material and smooth out any surface imperfections. Finally, the mounting holes are drilled out to allow for attachment to to sagittal motor and leg interface (Figure 3.8(f)). A more detailed procedure is given in Appendix B.

3.3   Interface Geometry and Adjustability

The exoskeleton can be adjusted to different user heights and widths as well as femur locations as shown in Figure 3.9. The current orthosis limits users to a certain range of body

17
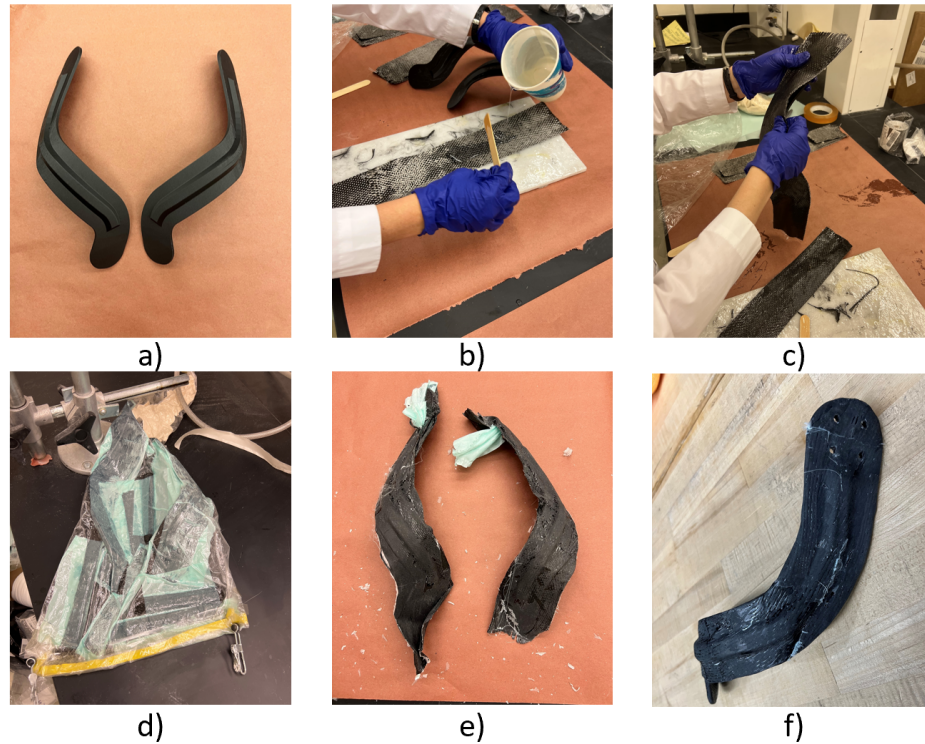
Figure 3.8: Leg strut reinforcement process. (a) Printed leg struts before reinforcement. (b) Applying epoxy solution to carbon fiber tape. (c) Laying carbon fiber tape of printed struts. (d) Vacuum packing of reinforced parts. (e) Reinforced parts before post-processing. (f) Final reinforced leg strut.

sizes but can be switched out for different sizes. From its central position, the frontal motor mount can be adjusted vertically ± 2 cm in 1 cm increments to adapt to different femoral head heights. The frontal motor mount comes in 3 sizes for the separation of the frontal actuators (168 mm, 178 mm, and 188 mm) to adapt to the different mediolateral hip joint center widths. The position of the sagittal motor is controlled by adjusting the mounting location of the aluminum rods in the L-junction assembly which allows the exoskeleton to adjust for different user hip widths and anteroposterior hip joint center positions. Currently, the exoskeleton accommodates hip widths ranging from 32-55 cm which represents a range from the lower 10% to upper 99% of the United States' population [29]. Finally, the exoskeleton has a range of motion more than enough to accommodate the user's movement during normal walking and perturbation recovery. The design allows for 95° flexion, 90° extension, 45° abduction, and 90° adduction which exceeds our ROM goals (section 2.2).
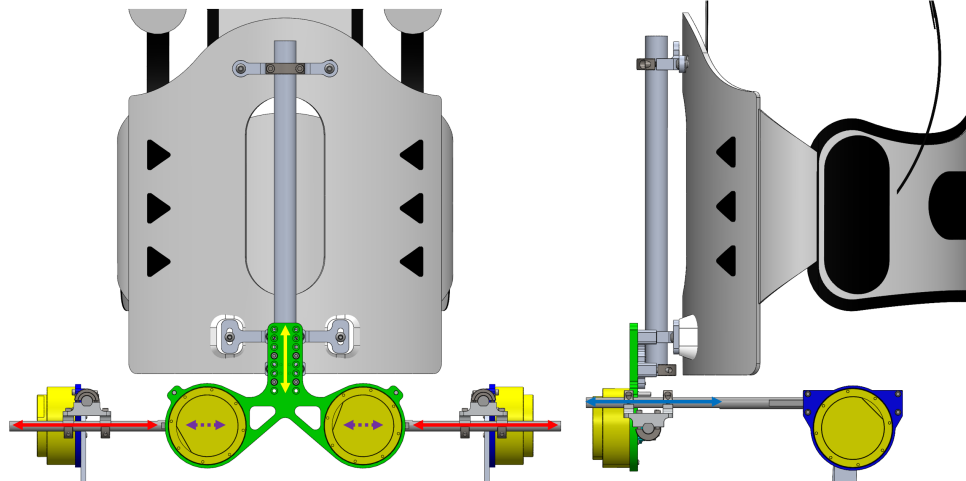
Figure 3.9: Adjustability of the exoskeleton. The design uses sliding on D-shaft rods to adjust the overall hip width (red) and anteroposterior hip joint center position (blue). The height of the hip joint center (yellow) is adjusted in 1 cm increments by the frontal motor mount location. Finally, the mediolateral hip joint center width (purple) is controlled by different sizes of frontal motor mounts.

3.4 Material Testing

A series of tensile material tests were performed to test the effect of the carbon fiber reinforcing process and to confirm that it is a viable replacement to traditional carbon fiber parts. The tensile tests produced stress-strain relationships that are used to estimate the ultimate tensile strength (UTS) and Young's modulus of the reinforced specimens. These values are needed for calculating the safety factor of the leg struts.

3.4.1 Methodology

Using the ASTM D790 standard, three onyx tensile specimens were reinforced, as described in subsubsection 3.2.3, and tested. Additionally, three onyx and ABS tensile specimens were tested to compare with the reinforced specimens. Standard tensile tests were performed with a strain rate of 15 mm/min and 100 mm initial separation on a Instron 5967 Universal Testing system.

3.4.2 Results

The results of the tensile tests (Table 3.2 and Figure 3.10) show that carbon fiber reinforcement significantly increases the specimens strength and stiffness. When taking into account the extra weight added by the reinforcement process, the reinforced specimens have a specific strength almost 15 times higher than the non-reinforced Onyx specimens. However, the reinforced specimens are only a fraction as strong and stiff as traditional carbon fiber composites even when taking into account weight. This is to be expected since much of the cross sectional area of the specimens is 3D Onyx.

Table 3.2: Tensile test results. Shows the average strain at ultimate tensile strength (UTS), UTS, modulus, and specific strength for the series of specimens tested. Traditional carbon fiber/epoxy composites were not tested but online reference data is included. Uncertainty range is 95% confidence interval.

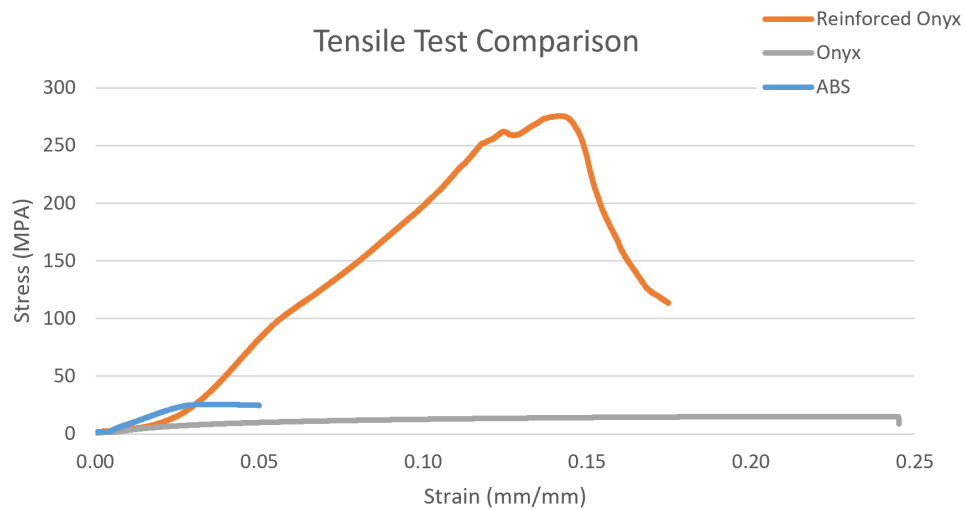| Specimen	Strain at UTS (mm/mm)	UTS (MPa)	Modulus (MPa)	Specific Strength (kNm/kg)
Reinforced	0.13±0.04	282±35	2,340±611	201.3±25.3
Onyx	0.22±0.03	15±0.3	160±13	14.0±0.2
ABS	0.04±0.00	25±0.1	879±143	17.5±0.2
Carbon Fiber Composite [32]	0.01	600	70,000	375

Figure 3.10: Tensile stress-strain graph comparison of reinforced and non-reinforced specimens. Each line represents the specimen that was closet to the average of the series.

While the results are promising, there are limitations with this data. The tensile specimens experienced failure in the grip area instead of the gauge area (Figure 3.11). This suggests that the testing specimens experienced premature failure due to stress concentrations located in the grip region of the specimens. These stress concentrations could have been caused by excessive clamping force or excessive material removal during reinforcement post-processing. Future tests are needed to determine how much stronger and stiffer the reinforced material is. Also, the lack in consistency in the orientation and placement of the carbon fiber tape as well as the extent of post processing removal may have led to the high amount of variability in the reinforced specimens compared to the non-reinforced ones. Furthermore, changing the shape and thickness of the part being reinforced will change its proprieties significantly since the carbon fiber is applied only on the surface of the 3D printed part. As a result, these numbers shouldn't be directly used for determining the strength of a reinforced part, rather, they serve as an indicator of the process's effectiveness.
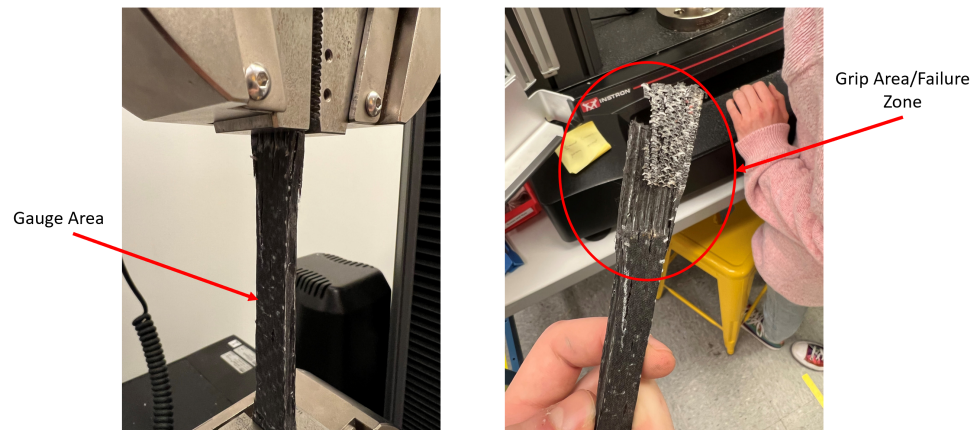

Figure 3.11: Failure mode of reinforced tensile specimens. All three reinforced specimens failed in in the top grip area. The grips seem to have over compressed on the specimen and stripped the carbon fiber tape at its breaking point.

3.5 Force Analysis and Safety Factors

The exoskeleton was designed so that the user would be safe while operating the device. All parts have smooth geometry to prevent sharp edges that could cut the user. The actuator is backdriveable and has a low peak torque relative to the average user's strength, which ensures that it would never force the user's movement. Nevertheless, hard stops are included in the frontal and sagittal plane to prevent excessive rotation. Finally, a goal safety factor of 2 was used for all components holding the motors. A safety factor of 1.7 was specified for the connector plate so that it would be more likely to fail before other components since it was deemed a safe location to fail.

To calculate the expected maximum stresses experienced by the individual components of the assembly, the expected maximum reaction forces were calculated based on the peak output torque of the actuators (24.8 Nm) and the location of the leg cuffs. Instead of being attached further along the leg, the leg cuffs attach at the user's lower thigh to minimize the forces being placed on the user's leg by the actuators. Given that the vertical separation of the leg struts is constant ($\approx$30 cm), the maximum expected reaction force on the leg would be $\approx$85 N in the sagittal and frontal planes without considering losses due to shear. These forces are transmitted through the rest of the design as shown in Figure 3.12. To maximize the stress exerted, the finite element analysis (FEA) simulations maximize the moment arms of leg cuff reaction forces acting on the individual components based on the limits of the design. Furthermore, the reaction forces occur in the worst directions for the component being analyzed so that they compound instead of canceling each other out. Additionally, a 50 N downwards force was added to each FEA simulation to represent an external bump from the user of the environment. The FEA simulation results for each component of the interface can be found in Appendix C. These FEA simulations allowed for weight saving features to be added without compromising the parts safety factors but more time could be spend on optimizing these features.
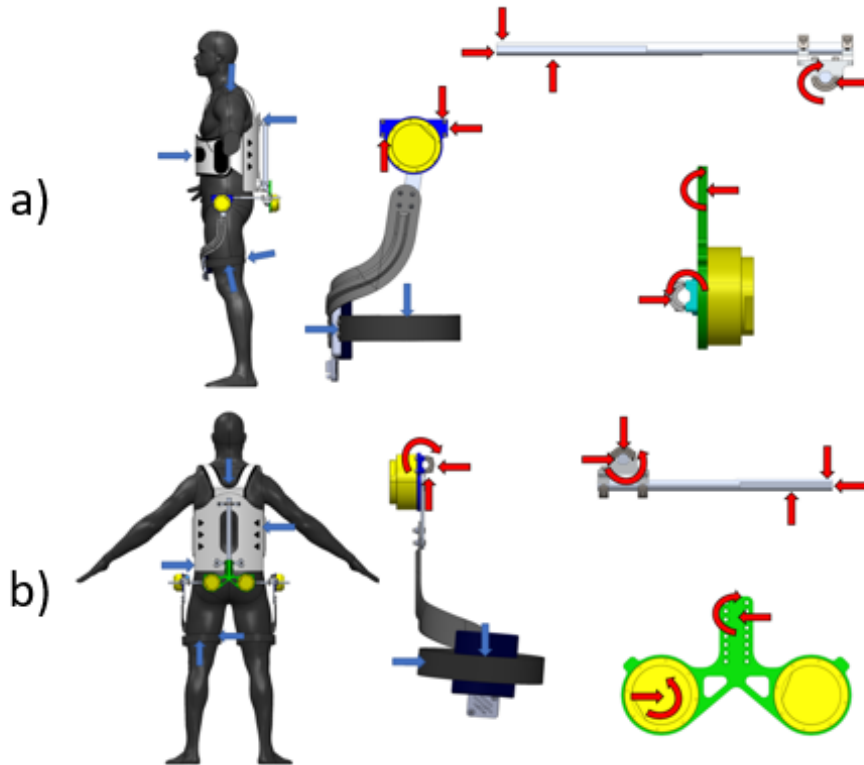
Figure 3.12: Reaction forces from hip flexion (a) and abduction (b). The blue arrows represent external forces while the red arrows represent how the forces are transmitted throughout different sections of the design.

3.5.1 Leg Strut Analysis

Creating a FEA for the leg strut posed a difficult problem since the exact properties of reinforced parts are difficult to deduce without material tests on said parts due to the composite nature of the material. Since the leg struts took significant time to make and said material testing would destroy any part tested, the material properties used for the FEA simulation are based off the reinforced specimen results showed in Table 3.2. More specifically, the lower end of the range of UTS and Young's modulus were used to create a custom material for the leg strut's FEA simulation. The compression tests required to calculate Poisson's ratio were not carried out; therefore, the FEA simulation uses the base material's (Onyx) Poisson's ratio of 0.104 [33] since it is the lowest possible Poisson's ratio and maximizes the stress calculated. For the FEA simulation, the leg strut's CAD model has its strengthen-

ing rib removed to make the part's thickness uniform throughout. This gives the simulation leg strut a rectangular cross section like the tensile testing specimens. With this and the fact that the reinforced leg strut has a similar thickness compared to the tensile test specimens (5.5 mm compared to ≈5.3 mm), it is reasonable to assume that the leg strut has similar mechanical properties to the tensile test specimens; however, removing the rib significantly reduces the rigidity and strength of the simulation leg strut.
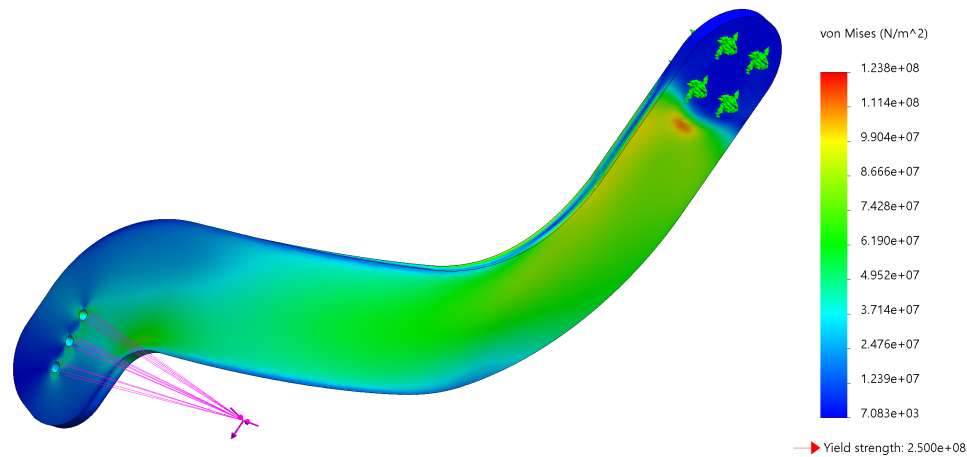
Figure 3.13: FEA simulation of reinforced leg strut. Subjected to 85 N in the lateral and anterior directions and well as a 50 N downwards force. Model is fixed at the connector plate interface. The maximum stress calculated by the simulation was 124 MPa which is roughly half the predicted tensile strength of the reinforced leg strut.

The leg struts FEA simulation has the same load scenario as the other exoskeleton components. The FEA simulation (Figure 3.13) shows that, with the assumptions made, the leg strut should have a safety factor of at least 2.0 with the expected loading case. The actual safety factor is probably significantly higher because of the strengthening ridge that was removed along with other conservative assumptions made.

3.6 Mass

Reducing the mass of this exoskeleton in comparison to previous designs is a goal for the design. The exoskeleton has a projected mass of 7.8 kg with mechatronics added (Table 3.3), and this is significantly lower than our limit of 9.0 kg. While most of the com-

ponents are designed to be lightweight, a few OTS components were used which did not prioritize reducing weight. Many steel shaft collar clamps are used throughout the design to secure the aluminum rods and altogether weighed around 0.7 kg. Aluminum shaft clamps could be designed to replace the steel version which could save around 0.5 kg. Furthermore, as mentioned before, the lumbar orthosis weighs 1.8 kg which is much more than what was originally planned. Unfortunately, a lighter weight alternative would be difficult to produce while maintaining the comfort and solid foundation provided by the orthosis.

Table 3.3: Mass estimates for different segments of the design. Structural mass are mostly based off CAD model. The OTS structural mass section represents structural components that were not custom made such as the lumbar orthosis. In turn, the structural mass and fasteners section represents the weight of all custom designed parts and the fasteners used. The mechatronics section represents an estimate for the added weight from batteries, sensors, and wiring.

	Actuators (kg)	OTS Structural Mass (kg)	Structural Mass and Fasteners (kg)	Mechatronics (kg)	Segment Mass (kg)
Back	0.0	2.0	0.3	0.8	**3.1**
Hip	2.0	0.5	1.7	0.1	**3.9**
Leg	0.0	0.0	0.7	0.1	**0.8**
Total	**2.0**	**2.5**	**2.8**	**1.0**	**7.8**

CHAPTER 4

DISCUSSION

This thesis covers the design and manufacturing of 2-DOF hip exoskeleton that is focused on assisting in gait stabilization. The design is lighter and more compliant than previous examples of 2-DOF hip exoskeletons. While further testing is needed, this exoskeleton will enable further studies on the effectiveness of exoskeleton assistance in improving gait stability.

The exoskeleton's actuators are QDD to allow for transparent assistance to the user by being backdriveable and they have a high torque to weight ratio to maximize the amount of assistance given to the user while staying lightweight. Previous perturbation studies suggested a maximum peak torque output of 250 Nm and 400 Nm for the frontal and sagittal plane actuators. The actuators for both planes of the hip only provide a peak torque output of 24.8 Nm due to the requirement to have low gearing and to minimize worn mass. While this is much less than ideal, there is evidence that lower levels of torque assistance can still help with balance recovery. One study on an metabolic-saving focused exoskeleton design found that a peak torque of 25 Nm applied to the hip sagittal plan during walking lead to significant improvements in energy cost [34], which suggests that a similar level of assistance could also help with a user's response to perturbations. Future experiments with the exoskeleton will test this hypothesis.

The ability of the exoskeleton to adjust to a wide range of hip joint locations and hip widths allows for a comfortable fit and effective torque transfer to a majority of the adult population. Aligning the actuators with the hip joints will be performed manually by researchers based on biological markers and therefore some misalignment is to be expected. Thankfully, previous exoskeleton designs have shown that only rough actuator alignment with the hip joint is needed for comfortable and effective assistance [12]. Whether or not

alignment is good enough is currently determined by verbal feedback from the user.

The 3D printed, carbon fiber reinforced leg struts proved to be a satisfactory prototyping alternative to traditionally made carbon fiber parts. Tensile tests on reinforced specimens showed a significant increase in specific strength and stiffness compared to their pre-reinforced state. However, there are some limitations. The surface finish and overall dimensional tolerances were negatively affected by the need for post-processing. Furthermore, the actual mechanical properties that come with reinforcement are highly dependent on the part being reinforced and the way carbon fiber tape is applied. Finally, the reinforced parts are weaker and more pliable than traditional carbon fiber parts. While they do not have as good mechanical properties, the reinforced parts in this paper are cheaper and quicker to produce than traditional carbon fiber parts. Most importantly, reiforced parts are strong and stiff enough for our application. Therefore, the reinforcement method used in this thesis is a promising way to either test out or even replace carbon fiber parts for prototyping.

The components of the exoskeleton are designed to safely handle up to 25 Nm from all actuators at once, but it is currently untested and, therefore, future adjustments (e.g. changes in geometry/material) may be needed once testing begins. One concern would be whether the aluminum adjustment rods would slip with higher torques. Chiu *et al.* experienced slipping on their adjustment rods at around 75 Nm even though they designed everything to go up to 100 Nm. While this is much more torque than our exoskeleton will experience, that example serves as a reminder that unforeseen changes might be necessary in response to problems that come up during testing.

With the mass of the exoskeleton coming in at 7.8 kg, the design is below our goal of 9 kg. While some mass reductions could be made by replacing OTS components with custom built designs, a full redesign using less conventional materials would be needed to make a significantly lighter 2-DOF hip exoskeleton with the selected actuators. First, more time could be spent on optimizing the weight saving features of the individual com-

ponents. Another possible method of reducing mass would be to expand the use of 3D printed reinforced parts to other areas of the design. The reinforced tensile specimens had a specific strength around double that of aluminum. However, their lack of dimensional accuracy limits their use to components that do not impact the orientation of the actuators. A more realistic but less practical option would be to use traditional carbon fiber parts. While this could decrease mass, excessive use of traditional carbon fiber parts is expensive. Finally, lighter actuators could be selected to reduce the overall design mass. This option is more practical as technology continue to improves; but any OTS actuator that weighs less than the one currently selected is currently expensive, does not have a large enough torque output, or is not QDD. While there is room for improvement in the future, altogether, the design's mass is still significantly lighter than previous 2-DOF exoskeletons (Zhang *et al*'s being 9.2 kg and Chiu *et al*'s being 10.9 kg) [14, 20].

Once equipped with mechatronics and live tested during steady human walking, this exoskeleton will go on to be used in tests during balance recovery perturbations. Future design work should focus on ways to lower the weight of the design while increasing the assistance torque. Furthermore, more analysis of the reinforced 3D printed parts is needed to capture their effectiveness. Finally, more research is needed to determine the effect of different levels of torque assistance in order to understand torque requirements for optimal exoskeleton gait stabilization assistance.

CHAPTER 5

CONCLUSION

The 2-DOF exoskeleton put forward in this thesis aims to assist in the user's gait stability. Actuation of hip flexion/extension as well as hip ad/abduction allows for active assistance in the sagittal and frontal plane. Backdrivable QDD motors are employed to allow for transparent motion when assistance is off. The exoskeleton, when the mechatronics are added, will have a projected mass of 7.8 kg which is lighter than previous published 2-DOF hip exoskeleton designs by 15%. Finally, this thesis explored an alternative to producing carbon fiber parts by reinforcing 3D printed leg struts. After testing the exoskeleton and making any necessary changes, future studies will use the exoskeleton to study the effect of assistance on gait stabilization.

Appendices

APPENDIX A

GAIT SCENARIOS

This appendix serves as further analysis on the AK70-10's estimated biological assistance for different gait scenarios. The assistance potential of the steady state (Figure A.1), slip perturbation (Figure A.2), and ML perturbation (Figure A.3) trial data sets are recalculated using Equation 2.1 without being furthered lowered by calculating the potential of overheating using Equation 2.2. This was to test the maximum assistance levels during the highest demand sections of the scenarios if the motor assistance was intermittent instead of consistent. Furthermore, the steady state and slip perturbation trials are limited to swing phase only to explore the potential maximum assistance during our target area of the gait cycle.

From these changes, only the slip perturbation study (Figure A.2) has a biological assistance level shown higher than the results shown in Figure 3.3, increasing from 13.4% to 26.2%. While further constraints may change the results, these new results show intermittent assistance during targeted areas of the gait cycle may not produce much higher assistance levels compared too consistent assistance throughout different scenarios. While swing phase requires less torque than stance phase, the increased rotational velocity needed for steady state gait during the swing phase raises the voltage needed to the AK70-10's limit over the stance phase (Figure A.1). Finally, the lack of increase in biological assistance for steady state and ML perturbation scenarios show that RMS torque was not a limiting factor in maximum biological assistance.
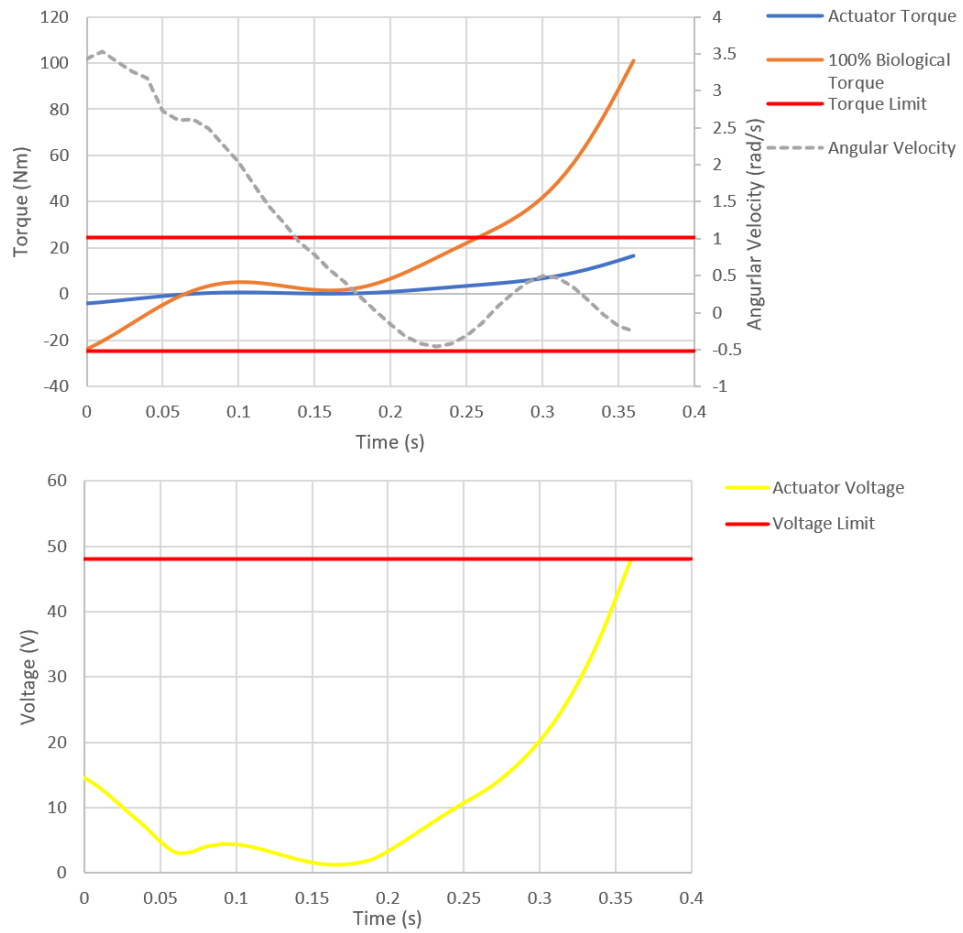
Figure A.1: AK70-10 simulation for sagittal steady state hip torque during swing state. Torque and voltage limits represent the nominal limits of the AK70-10. The actuator is able to provide 16.6% biological assistance according to Equation 2.1. Data taken from [25].
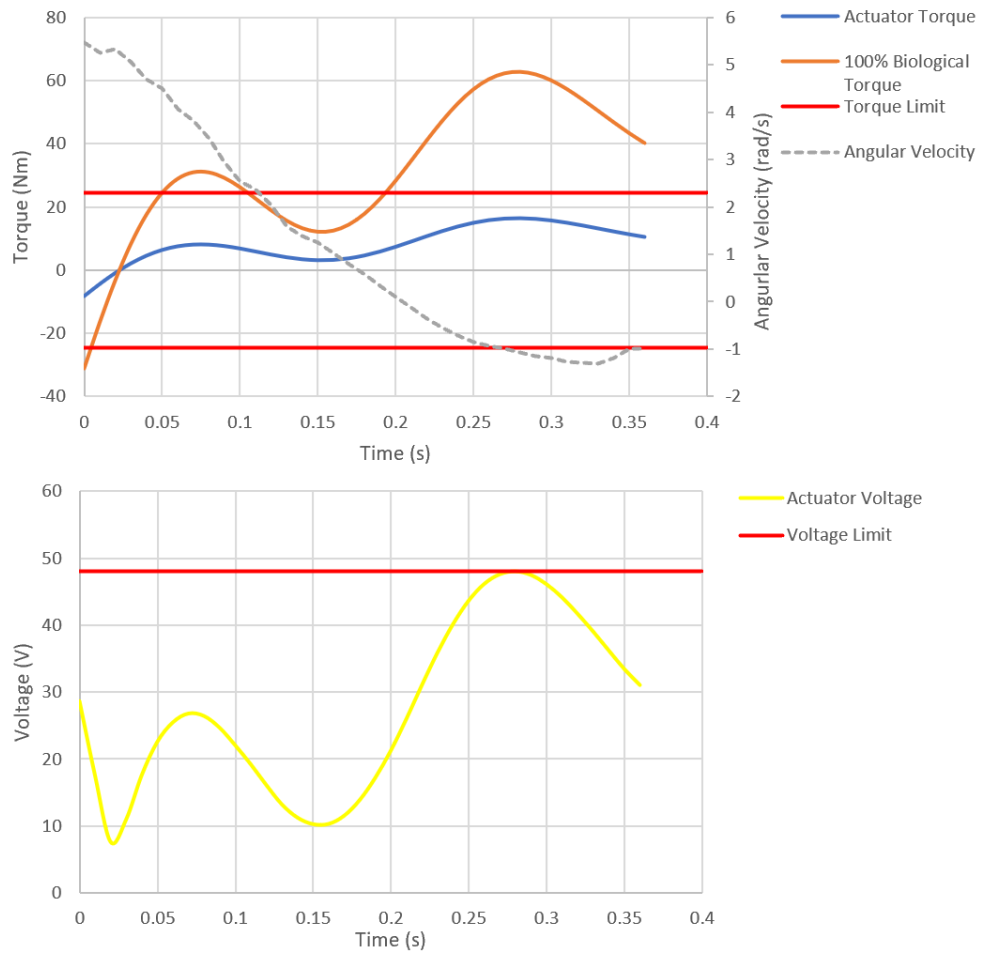
Figure A.2: AK70-10 simulation for sagittal slip perturbation hip torque during swing state. Torque and voltage limits represent the nominal limits of the AK70-10. The actuator is able to provide 26.2% biological assistance according to Equation 2.1. Data taken from [25].
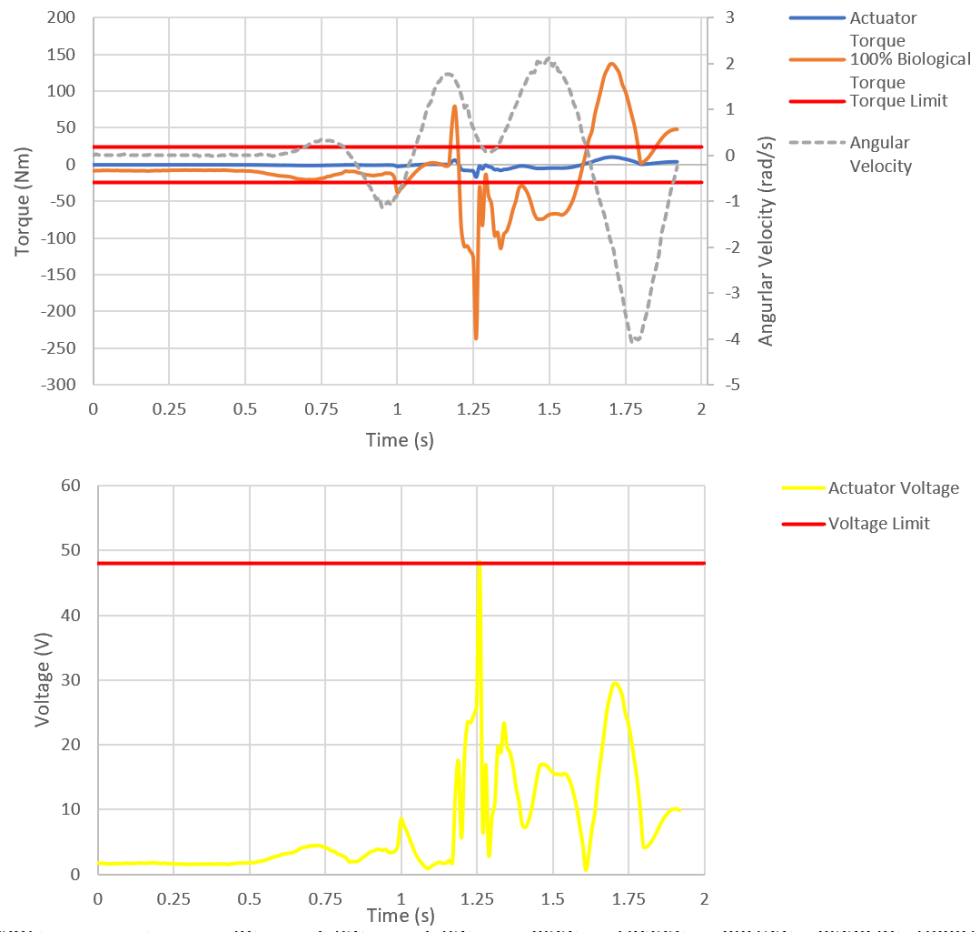
Figure A.3: AK70-10 simulation for frontal ML perturbation hip torque. Torque and voltage limits represent the nominal limits of the AK70-10. The actuator is able to provide 7.1% biological assistance according to Equation 2.1. Data taken from [23].

APPENDIX B

DETAILED REINFORCEMENT PROCESS

This appendix covers a detailed description of how to reinforce 3D printed parts with carbon fiber tape.

B.1   Supplies Needed

Uni directional carbon fiber tape (3" wide in my case), epoxy resin kit (Resin A and Resin B), 3d printed part, nylon rag, PVA bag, yellow sealant tape, peal ply (optional), normal tape, plastic cup, popsicle stick, scissors, and clamps.

B.2   Process

1. 3D Printed Part

   - Make sure that the part that you are reinforcing isn't too big for your PVA bag and that you have a good width tape to reinforce each side with.

2. Lab Prep

   - Besides making sure you have everything, there are some things you can do before going to the lab to save some time for anyone helping you.

   - You want to make sure the surface of your part isn't smooth so that the epoxy resin will stick to the surface. Use a file or some sandpaper to rough up the surface.

   - Cut the carbon fiber tape to the length you want so that it can cover your part longitudinally. Make sure you cut enough to reinforce each part on each side by the amount of layers you want

3. PVA Bag Prep

   - Soak a towel in the sink and then ring it out to get rid of excess water. Lay it on the table and put the PVA bag in it as shown. Roll up the towel and PVA bag like a burrito and let it set for 6 minutes.

4. PVA Attachment

   - After 6 minutes, remove the bag from the towel and attach the narrow end to the vacuum tube. Rap the attachment point with tape to ensure it's an air tight fit. Stick a nylon rag in the bag all the way to the vacuum tube. This will prevent epoxy resin getting into the vacuum generator and is therefore really important!

5. Resin Mixing

   - Before doing this, make sure you have everything ready for the following steps. Once the resin is mixed you shouldn't waste too much time as the resin may start to set and negatively affect the quality of the reinforcement. Put your respirator and gloves on and keep them on until you are past step 7. The resin kit we had had two different components that were mixed together. The proportions you use will be based off the epoxy resin kit you have so read those instruction. Use the scale in the plastic bag to weight the cup as you add things to make sure the proportions are correct. Lightly mix with a popsicle stick to prevent too much air mixing in.

6. Lamination

   - Have all the cut pieces of tape ready for one part. If you are using peal ply, cut enough pieces that can cover each side of the part.

   - Put a sheet of paper on the table next to the lamination bag and get the sticky board pictured. Put a piece of carbon fiber tape on the board and pour a bit of

resin mixture on it, and use a popsicle stick to spread the resin out. Repeat this on the other side of the tape so it's nice and lathered.

- Apply the lathered carbon fiber tape longitudinally to one side of the 3d print. Manipulate the tape so that it follows the curves of the part. Repeat this until you have the number of layers you want on one side of the part before doing the same amount of layers on the other side.

- Put one layer of peal ply on the part on each side just like the carbon fiber tape.

- Put the part into the PVA bag.

- Repeat the previous steps for each part that you are reinforcing. Try to spread the parts out so there isn't much overlap.

7. PVA Bag Sealing

- With all the parts in the bag, roll up the open end of the PVA bag. Turn on the vacuum on to take all the air out of the bag. Apply sealant tape to the opening of the PVA bag that's rolled up. Fold the PVA bag over the yellow tape and put some clamps on at the corner to keep it in place. Apply normal tape over the fold for extra sealing. During anytime in this process you can smooth out the folds in the PVA bag to improve the surface finish. At this point you are basically done, leave the vacuum on. You can remove your respirator and clean up. Come back the next day.

8. Post Processing

- After giving the part a day to set, you will be able to come in and remove all the parts from the PVA bag. The edges will have to be smoothed out with a grinder. Once it looks like its supposed to, go over it with sandpaper. If there are any holes in the the parts where carbon fiber tape doesn't cover it just redo the process but only for the uncovered parts.

APPENDIX C

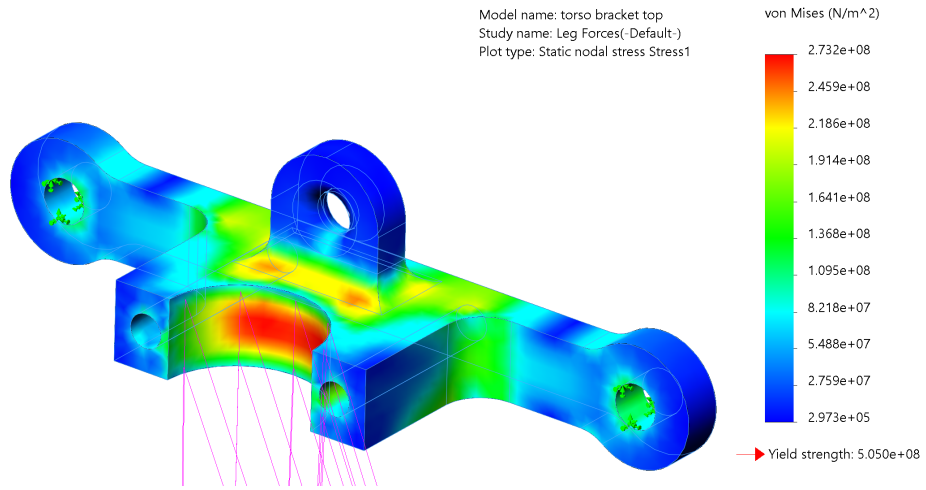# FINITE ELEMENT ANALYSIS

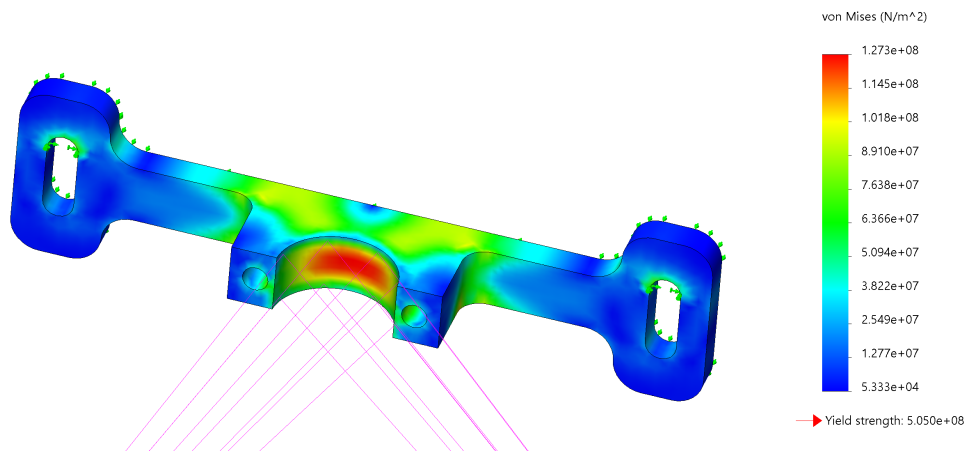Figure C.1: Torso bracket top FEA.

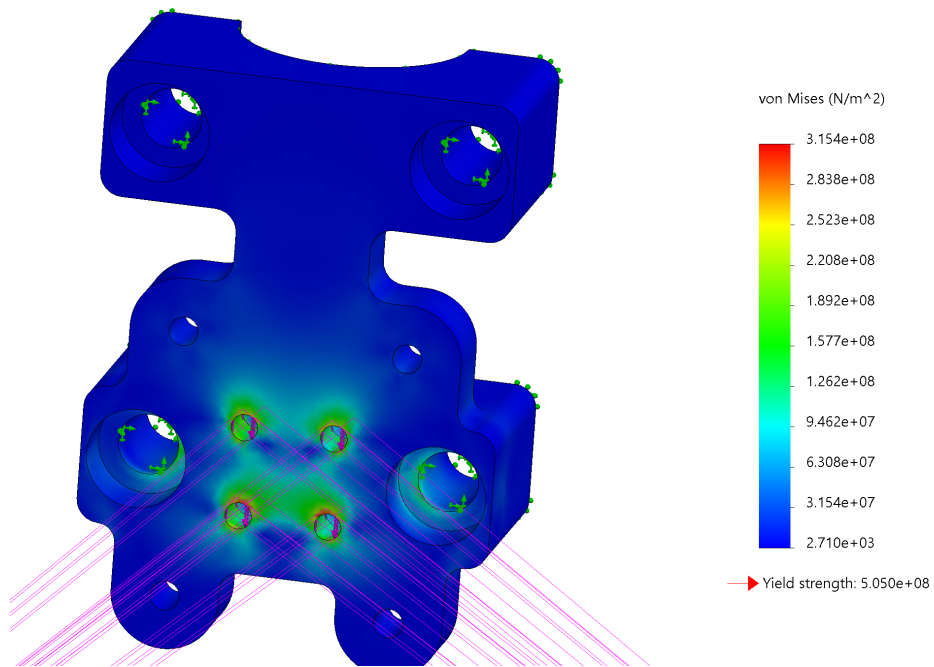Figure C.2: Torso bracket bottom FEA.

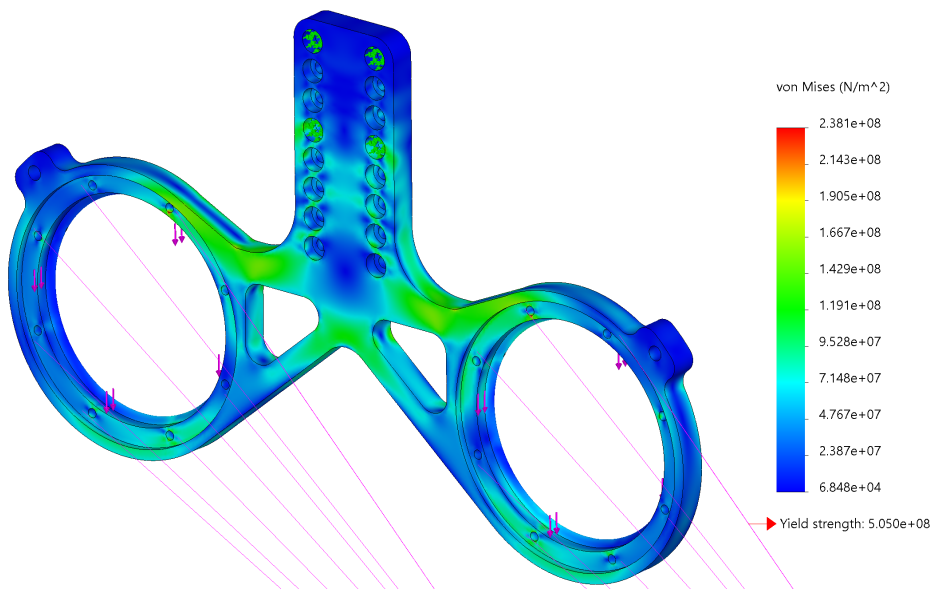Figure C.3: Back Interface Connector FEA
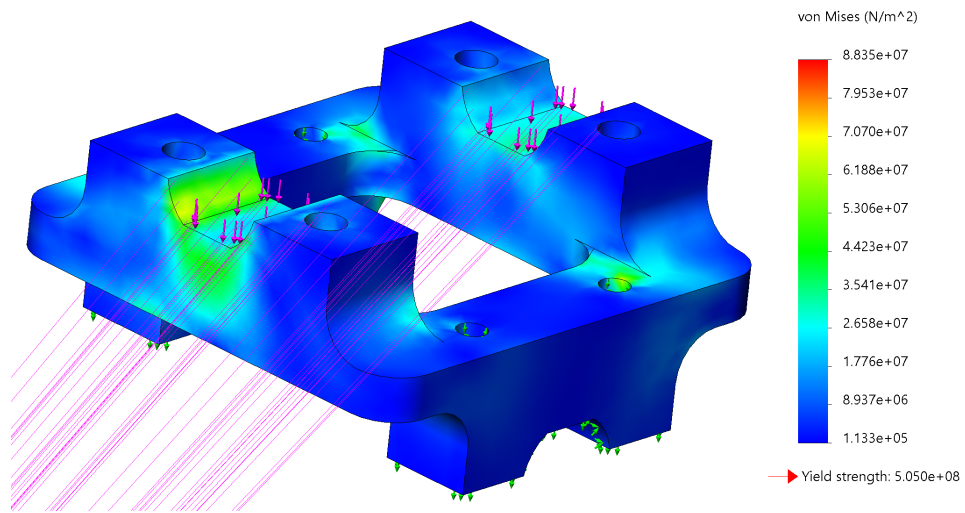

Figure C.4: Sagittal motor mount FEA.

Figure C.5: L-junction FEA.
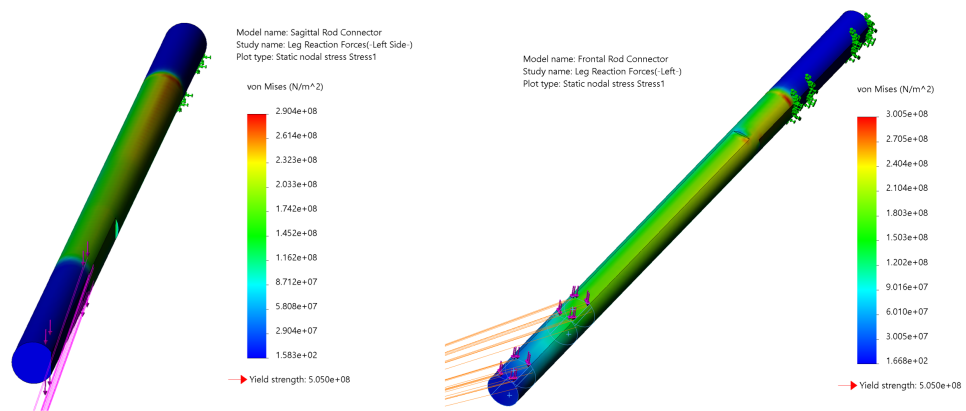
Figure C.6: Sagittal and frontal rod connector FEA.

Figure C.7: Sagittal Motor Mount FEA.
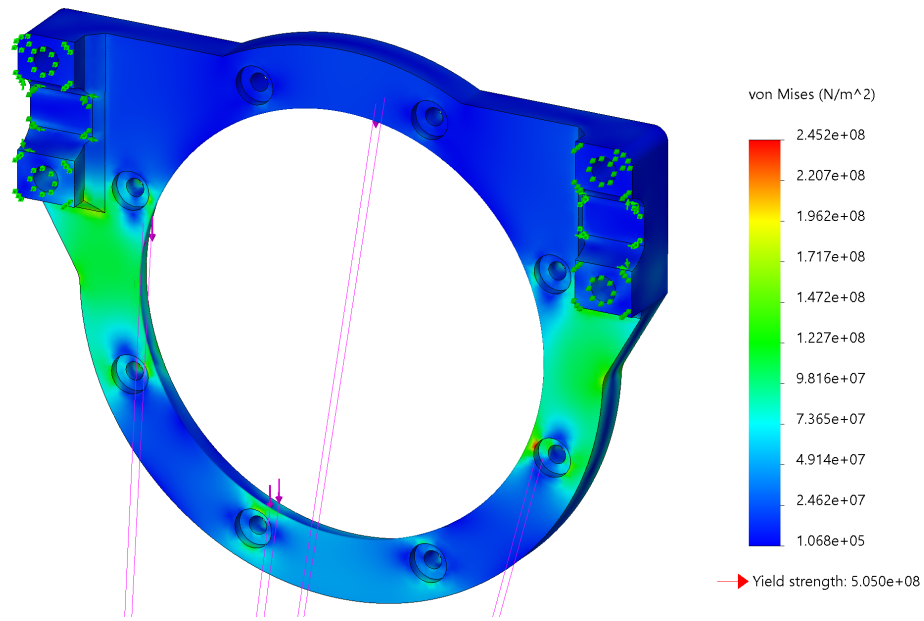
Model name: ConnectorLegBar
Study name: Leg Reaction Forces(-Default-)
Plot type: Static nodal stress Stress1
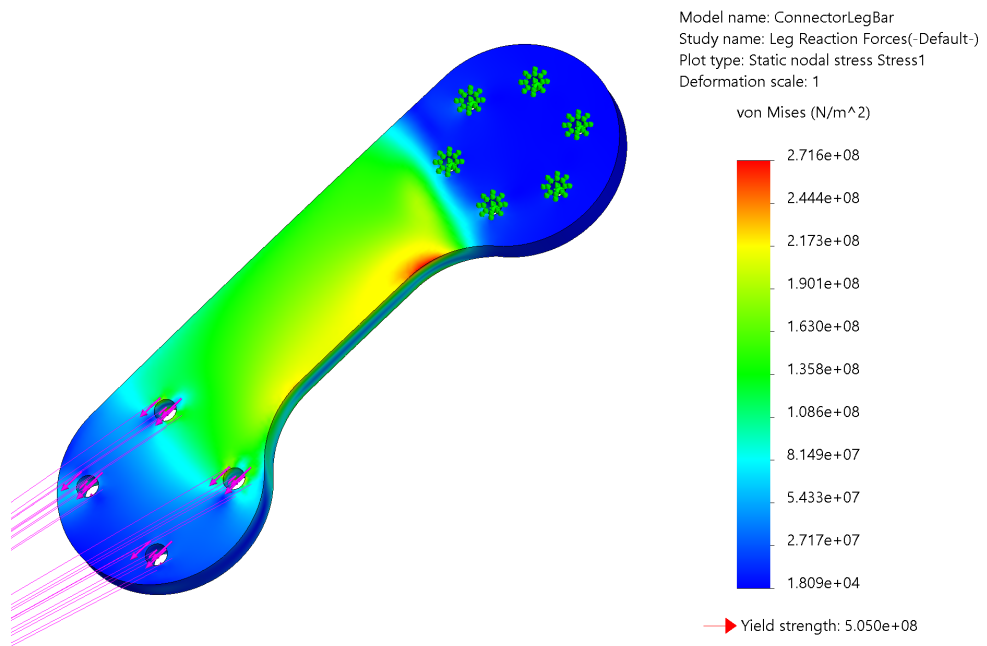Deformation scale: 1

Figure C.8: Leg bar connector FEA.

REFERENCES

[1] J. M. Hausdorff, D. A. Rios, and H. K. Edelberg, "Gait variability and fall risk in community-living older adults: A 1-year prospective study," *Archives of Physical Medicine and Rehabilitation*, vol. 82, no. 8, pp. 1050–1056, Aug. 2001.

[2] L. M. Wagner, V. L. Phillips, A. E. Hunsaker, and P. G. Forducey, "Falls among community-residing stroke survivors following inpatient rehabilitation: A descriptive analysis of longitudinal data," *BMC Geriatrics*, vol. 9, no. 1, 2009.

[3] W. E. Wei *et al.*, "Post-stroke patients with moderate function have the greatest risk of falls: A National Cohort Study," *BMC Geriatrics*, vol. 19, no. 1, Dec. 2019.

[4] G. Birhanie, H. Melese, G. Solomon, B. Fissha, and M. Teferi, "Fear of falling and associated factors among older people living in Bahir Dar City, Amhara, Ethiopia- a cross-sectional study," *BMC Geriatrics*, vol. 21, no. 1, Dec. 2021.

[5] Q. Wu, X. Wang, F. Du, and X. Zhang, "Design and control of a powered hip exoskeleton for walking assistance," *International Journal of Advanced Robotic Systems*, vol. 12, Mar. 2015.

[6] I. Kang, H. Hsu, and A. Young, "The Effect of Hip Assistance Levels on Human Energetic Cost Using Robotic Hip Exoskeletons," *IEEE Robotics and Automation Letters*, vol. 4, no. 2, Apr. 2019.

[7] F. Giovacchini *et al.*, "A light-weight active orthosis for hip movement assistance," in *Robotics and Autonomous Systems*, vol. 73, Elsevier B.V., Nov. 2015, pp. 123–134.

[8] C. McCrum, M. H. Gerards, K. Karamanidis, W. Zijlstra, and K. Meijer, "A systematic review of gait perturbation paradigms for improving reactive stepping responses and falls risk among healthy older adults," *European Review of Aging and Physical Activity*, vol. 14, no. 1, Mar. 2017.

[9] F. B. Horak, "Postural orientation and equilibrium: what do we need to know about neural control of balance to prevent falls?" *Age and Ageing*, pp. 7–11, 2006.

[10] G. S. Sawicki, O. N. Beck, I. Kang, and A. J. Young, "The exoskeleton expansion: Improving walking and running economy," *Journal of NeuroEngineering and Rehabilitation*, vol. 17, no. 1, Feb. 2020.

[11] I. Kang, D. D. Molinaro, S. Duggal, Y. Chen, P. Kunapuli, and A. J. Young, "Real-Time Gait Phase Estimation for Robotic Hip Exoskeleton Control During Multi-

modal Locomotion," *IEEE Robotics and Automation Letters*, vol. 6, no. 2, p. 3491, 2021.

[12] G. M. Bryan, P. W. Franks, S. C. Klein, R. J. Peuchen, and S. H. Collins, "A hip–knee–ankle exoskeleton emulator for studying gait assistance," *International Journal of Robotics Research*, vol. 40, no. 4-5, pp. 722–746, Apr. 2021.

[13] R. J. Van Arkel, A. A. Amis, J. P. Cobb, J. R. T. Jeffers, J. R. T. Jeffers, and. J. P. Cobb, "The capsular ligaments provide more hip rotational restraint than the acetabular labrum and the ligamentum teres," *The Bone & Joint Journal*, Nov. 2014.

[14] V. L. Chiu, M. Raitor, and S. H. Collins, "Design of a Hip Exoskeleton With Actuation in Frontal and Sagittal Planes," *IEEE Transactions on Medical Robotics and Bionics*, vol. 3, no. 3, pp. 773–782, Jun. 2021.

[15] S. M. O'connor and A. D. Kuo, "Direction-Dependent Control of Balance During Walking and Standing," *J Neurophysiol*, vol. 102, pp. 1411–1419, 2009.

[16] D. Conradsson, C. Paquette, and E. Franzé, "Medio-lateral stability during walking turns in older adults," *PLOS One*, 2018.

[17] P.-C. Kaoid and S. Srivastava, "Mediolateral footpath stabilization during walking in people following stroke," *PLOS One*, Nov. 2018.

[18] J. C. Singer, S. D. Prentice, and W. E. McIlroy, "Age-related changes in mediolateral dynamic stability control during volitional stepping," *Gait & Posture*, vol. 38, no. 4, pp. 679–683, Sep. 2013.

[19] S. Wang *et al.*, "Design and Control of the MINDWALKER Exoskeleton; Design and Control of the MINDWALKER Exoskeleton," *IEEE Transactions on Neural Systems and Rehabilitation Engineering*, vol. 23, no. 2, p. 277, 2015.

[20] T. Zhang, M. Tran, and H. Huang, "Design and experimental verification of hip exoskeleton with balance capacities for walking assistance," *IEEE/ASME Transactions on Mechatronics*, vol. 23, no. 1, pp. 274–285, Feb. 2018.

[21] G. A. Pratt and M. M. Williamson, "Series Elastic Actuators," *IEEE*, 1995.

[22] S. Yu *et al.*, "Quasi-Direct Drive Actuation for a Lightweight Hip Exoskeleton With High Backdrivability and High Bandwidth," *IEEE/ASME Transactions on Mechatronics*, vol. 25, no. 4, 2020.

[23] P. R. Moolchandani, A. Mazumdar, and A. J. Young, "Design of an Intent Recognition System for Dynamic, Rapid Motions in Unstructured Environments," *ASME Letters in Dynamic Systems and Control*, vol. 2, no. 1, Jan. 2022.

[24] J. M. Burnfield, K. R. Josephson, C. M. Powers, and L. Z. Rubenstein, "The influence of lower extremity joint torque on gait characteristics in elderly men," *Archives of Physical Medicine and Rehabilitation*, vol. 81, no. 9, pp. 1153–1157, Sep. 2000.

[25] P. R. Golyski, E. Vazquez, J. K. Leestma, and G. S. Sawicki, "Onset timing of treadmill belt perturbations influences stability during walking," *Journal of Biomechanics*, vol. 130, p. 110 800, Jan. 2022.

[26] D. J. Rutherford and C. Hubley-Kozey, "Explaining the hip adduction moment variability during gait: Implications for hip abductor strengthening," *Clinical Biomechanics*, vol. 24, no. 3, pp. 267–273, Mar. 2009.

[27] M. L. Mille, M. E. Johnson, K. M. Martinez, and M. W. Rogers, "Age-dependent differences in lateral balance recovery through protective stepping," *Clinical Biomechanics*, vol. 20, no. 6, pp. 607–616, Jul. 2005.

[28] D. V. Gealy *et al.*, "Quasi-Direct Drive for Low-Cost Compliant Robotic Manipulation," *ICRA*, vol. 1, pp. 437–443, 2019.

[29] C. C. Gordon *et al.*, "2012 Anthropometric Survey of U.S. Army Personel: Methods and Summary Statistics," Tech. Rep., 2014.

[30] M. Duarte, C. A. Fukuchi, and R. K. Fukuchi, "A public dataset of overground and treadmill walking kinematics and kinetics in healthy individuals," *PeerJ*, 2018.

[31] V. Elkarif, L. Kandel, D. Rand, I. Schwartz, A. Greenberg, and S. Portnoy, "Kinematics following gait perturbation in adults with knee osteoarthritis: Scheduled versus not scheduled for knee arthroplasty," *Gait & Posture*, vol. 81, pp. 144–152, Sep. 2020.

[32] Goodfellow, *Carbon / Epoxy Composite Materials - Properties*, May 2003.

[33] F. Ghebretinsae, O. Mikkelsen, and A. D. Akessa, "Strength analysis of 3D printed carbon fibre reinforced thermoplastic using experimental and numerical methods," in *IOP Conference Series: Materials Science and Engineering*, vol. 700, IOP Publishing Ltd, Nov. 2019.

[34] P. Franks, G. Bryan, R. Martin, and R. Reyes, "Comparing optimized exoskeleton assistance of the hip, knee, and ankle in single and multi-joint configurations," *Wearable Technologies*, vol. 2, no. 16, 2021.